Single-nuclear transcriptomics of lymphedema-associated adipose reveals a pro-lymphangiogenic stromal cell population

Gregory P. Westcott[1,5,*], Margo P. Emont[1,†], Anton Gulko[1], Zhibo Zhou[1], Charissa Kim[3], Gopal Varma[3], Leo L. Tsai[3,4], Eliza O'Donnell[1], Zinger Yang Loureiro[1], Wenle Liang[1], Christopher Jacobs[1,6], Linus T. Tsai[1,5], Timothy P. Padera[4,5], Dhruv Singhal[2,5], and Evan D. Rosen[1,5,6,*]

[1]Division of Endocrinology, Diabetes, and Metabolism, [2]Division of Plastic and Reconstructive Surgery, and [3]Department of Radiology, Beth Israel Deaconess Medical Center, Boston, MA

[4]Edwin L. Steele Laboratories, Department of Radiation Oncology, Massachusetts General Hospital Cancer Center, Massachusetts General Hospital, Boston, MA

[5]Harvard Medical School, Boston, MA

[6]Broad Institute, Cambridge, MA

[†]Current affiliation: Biological Sciences Division, University of Chicago, Chicago, IL

*Corresponding authors

Address correspondence to:
Gregory P. Westcott, MD
gwestcot@bidmc.harvard.edu

Evan D. Rosen, MD PhD
erosen@bidmc.harvard.edu

Word count: 3,184 (excluding abstract)

Key words: lymphedema, adipose tissue, lymphatic vessels, blood vessels, lymphangiogenesis, single-nucleus RNA sequencing

Abstract: Chronic lymphedema is a progressive, disfiguring disease that results from dysfunction of the lymphatic vasculature, causing distal accumulation of interstitial fluid, localized development of tissue edema, and expansion of subcutaneous adipose tissue (SAT). As the molecular mechanisms governing SAT remodeling in this disease are unclear, we performed single-nucleus RNA sequencing on paired control and affected SAT biopsies from patients with unilateral lymphedema. Lymphedema samples were characterized by expansion of SAA$^+$ adipocytes, pro-adipogenic stem cells, and proliferation of lymphatic capillaries. A *GRIA1*$^+$ lymphedema-enriched stromal cell population expressing *VEGFC*, *ADAMTS3*, and *CCBE1* was identified, suggesting an enhanced axis of communication between adipose stem and progenitor cells (ASPCs) and lymphatic endothelial cells. Furthermore, lymphedema ASPC-conditioned media promoted lymphatic endothelial tube elongation *in vitro*. These findings indicate a critical role for ASPCs in regulating adipocyte differentiation and lymphatic vascular remodeling in lymphedema, and provide a valuable resource for better understanding this disease.

Lymphedema is a progressive condition that results from impaired lymphatic drainage of the subcutaneous interstitial compartment, leading to fluid accumulation localized to the distal anatomic region[1]. With chronic lymphatic insufficiency, adipose differentiation takes place in the affected distribution[2], rendering the swelling irreversible, negatively impacting quality of life[3] and predisposing to other skin complications such as recurrent infection[4]. In developed regions, lymphedema is most often a complication of surgical lymphadenectomy or radiation for cancer treatment, affecting at least 20% of women undergoing treatment for breast cancer[5]. Worldwide, filariasis infection is the most prevalent etiology[6]. Obesity is also an increasingly common risk factor for lymphedema[7], particularly when the body mass index surpasses 40 kg/m^2. Despite a worldwide prevalence estimated at 140-250 million[6], there are limited non-surgical options to prevent, slow, or reverse lymphedema. Adjunctive medical approaches, such as VEGF-C-based adenoviral therapy[8] or administration of the leukotriene

B4 inhibitor ketoprofen[9], have failed to show improvement in lymphedema volume or lymphoscintigraphy parameters, highlighting the urgent need for novel therapeutic targets to address the primary burden of disease.

SAT expansion that occurs in chronic lymphedema confers much of the symptomatic disease burden and reflects the complex relationship between the lymphatic system and adipocyte differentiation and function[10,11]. In order to better characterize the complex interplay of diverse cell types and their role in lymphedema tissue remodeling, we performed single-nucleus RNA sequencing (sNuc-seq) on lymphedema-associated SAT, an approach we have previously used to construct a detailed atlas of human and mouse adipose tissue[12]. We also took advantage of the unilateral nature of localized limb lymphedema to obtain both affected and control samples from corresponding sites of the same subject, eliminating the confounding effects conferred by comparing two separate groups of individuals, and significantly improving our power to detect subtle differences between groups. Furthermore, sNuc-seq allows for the sequencing of mature adipocytes and the improved recovery of endothelial populations when compared to whole-cell sequencing technologies[12]. Our sequencing data and subsequent experimental studies indicate a role for adipose stem and progenitor cells (ASPCs) in coordinating both adipocyte differentiation as well as lymphatic capillary remodeling.

Results

Single-nucleus RNA sequencing atlas of lymphedema-associated SAT

Subjects with unilateral, chronic, fat-dominant lymphedema undergoing debulking surgery were recruited pre-operatively from the Beth Israel Deaconess Medical Center Department of Plastic and Reconstructive Surgery. Paired SAT biopsies were obtained from corresponding sites on the lymphedematous and unaffected (control) limbs from seven subjects for sNuc-seq, and lipoaspirate was collected from lymphedema and control subjects for ASPC isolation (**Fig. 1a**). See **Supplementary Table 1** for additional subject details. Magnetic resonance imaging (MRI) features were determined via

intensity-based threshold segmentation at the approximate location of each biopsy, and revealed expected increases in total subcutaneous area, subcutaneous fat, and interstitial fluid cross-sectional area in lymphedema (**Fig. 1b-c** and **Supplementary Table 2)**. The ratio of fat to total volume was lower in lymphedematous limbs, reflecting the increased fluid component due to impaired lymphatic clearance.

En bloc biopsies were processed for sNuc-seq (excluding skin) and histology (**Fig. 1d-e**). A total of 23,777 cells (10,785 control and 12,992 lymphedema) were identified in the sNuc-seq dataset, which includes all expected major adipose tissue cell types (**Fig. 1f-g**). Notably, there was a relative increase in vascular cells in lymphedema samples, reflected by an increase in blood and lymphatic endothelial cells as well as smooth muscle cells, while ASPCs, adipocytes, and macrophages decreased in proportion (**Fig. 1h**).

Lymphedema is characterized by expansion of an SAA^{+} adipocyte population

Adipocytes were assigned to seven subpopulations and labeled according to mapping with previously-defined subcutaneous human adipocyte subclusters[12] (**Fig. 2a-c and Extended Data Fig. 1a**). While Ad1, Ad2, and Ad3 did not contain highly-expressed transcriptional markers to differentiate them from other subpopulations, other clusters were more distinct. Ad^{ADGRB3} is a small population that expresses adhesion G protein-coupled receptor B3 (also known as brain angiogenesis inhibitor-3, *BAI3*), which was recently noted to have a role in adaptive thermogenesis[13]. Ad^{SAT1} expresses spermidine/spermine N1-acetyltransferase 1, which performs polyamine catabolism required for adipocyte thermogenesis; knockout of *Sat1* in adipocytes results in obesity[14]. Ad^{ITGBL1} expresses integrin-β–like 1, an integrin inhibitor that promotes chondrogenesis, as well as collagen gene *COL6A2*.

Ad^{SAA} was of particular interest, as this subpopulation is significantly greater as a proportion of adipocytes in lymphedema (23.5%) compared to control (11.1%) (p = 0.013) (**Fig. 2b** and **Extended Data Fig. 1b**). Ad^{SAA} expresses acute phase serum amyloid A isoforms *SAA1* and *SAA2* (**Extended**

Data Fig. 1c), which are apolipoproteins that are upregulated with increasing adipocyte size[17,18] in obesity[15] and during adipogenesis[16]. These serum amyloid A isoforms may play a role in cholesterol efflux to macrophages from hypertrophied adipocytes[17]. An adipogenesis gene signature (Hallmark Adipogenesis[19]) was applied to adipocyte and ASPC populations to assess the degree of differentiation[20], identifying Ad^{SAA} as the most differentiated adipocyte subpopulation (**Fig. 2d**). These findings are consistent with the presence of ongoing adipocyte differentiation and an increased overall adipocyte adipogenesis score in lymphedema across all individuals (**Fig. 2e** and **Extended Data Fig. 1d**).

Adipocyte size was measured in paired biopsy samples from three subjects on H&E images and confirmed with a fourth subject using BODIPY staining of whole mounted samples. In all subjects, average adipocyte size was decreased in lymphedema (**Fig. 2f-h** and **Extended Data Fig. 1e**). The literature describing adipocyte size in lymphedema is mixed, with some studies finding larger adipocytes in lymphedema[21,22], while others found no difference[23] or a higher proportion of hypertrophied adipocytes in non-lymphedema SAT[24], similar to our results. The presence of smaller adipocytes suggests the increase in fat volume is driven by substantial adipocyte hyperplasia and ongoing progenitor differentiation into newly-formed adipocytes.

Lymphedema-associated ASPCs increase proliferative gene expression and exhibit advanced adipogenic potential

In order to further investigate the response of adipocyte progenitors to lymphedema, ASPCs were subclustered into six populations (**Fig. 2i-k** and **Extended Data Fig. 1f-g**). $ASPC^{NAMPT}$ is characterized by expression of the NAD+ synthesis enzyme nicotinamide phosphoribosyltransferase, which has been implicated in adipose tissue plasticity and insulin resistance[25–27], as well as by expression of a number of collagen genes. $ASPC^{CD81}$ expresses CD81, indicating it could represent a beige adipocyte progenitor population[28]. $ASPC^{CD55}$ represents early progenitor cells expressing dipeptidyl peptidase 4

(*DPP4*) and *CD55*[29]. ASPC^{PTCH2}, which increased modestly from 7.9% to 11.9% in lymphedema, expresses hedgehog receptor patched 2 and shares transcriptional features with anti-adipogenic Aregs[30]. Notably, lymphedema is characterized by the dramatic increase in ASPC^{GRIA1}; ASPC^{GRIA1} is enriched for expression of the essential lymphangiogenic ligand *VEGFC* and the surface receptor glutamate receptor 1 (*GRIA1*).

Like adipocytes, ASPCs expressed a significantly higher adipogenesis signature in lymphedema (**Fig. 2l** and **Extended Data Fig. 1c**), consistent with a predisposition toward adipocyte differentiation. Most subpopulations of ASPCs also exhibited an increased stem cell proliferation signature (**Fig. 2d**). In order to assess whether ASPCs from lymphedematous regions exhibit enhanced cell-autonomous pro-adipogenic capacity, *in vitro* adipogenic differentiation was performed on isolated ASPCs from lymphedema and control subjects. Lymphedema-associated ASPCs differentiated more readily with standard adipogenic media both with or without addition of thiazolidinedione (**Fig. 2n-m**), consistent with other studies[31,32]. One report of equivalent adipogenic differentiation capacity in lymphedema[24] may reflect the use of a thiazolidinedione in all tested conditions, which, due to its potent PPARγ agonism, can mask subtle differences in inherent adipogenic potential.

ASPCs upregulate a subset of genes that correlate with disease severity and demonstrate augmented WNT, IGF, and BMP signaling in lymphedema

To further characterize the ASPC response to lymphedema, pseudobulk analysis was performed. In order to mitigate variability related to cell subsampling, pseudobulk was run 10,000 times, and differentially expressed genes (DEGs) that met significance in 90% of iterations were selected for further analysis (**Fig. 3a**). Pearson correlation coefficients were determined between DEGs and MRI characteristics to identify genes associated with disease severity, and subsets of genes that correlated with subcutaneous fat volume, fluid volume, or total volume were identified (**Fig. 3b**). ASPC1 displayed upregulation of genes that were positively associated with both fluid and fat volume, while ASPC^{NAMPT}

preferentially upregulated fluid-associated genes, and ASPC^{GRIA1} upregulated fat-associated genes (**Fig 3c**). ASPC subpopulations therefore may play unique roles in responding to interstitial fluid accumulation and mediating the natural history of lymphedema.

NicheNet[33] was applied to the gene expression profiles of ASPC subpopulations to model intercellular communication and identify regulatory signaling pathways. The top induced signaling pathways in lymphedema included *WNT1*, *NTF4*, *IGF2*, *BMP2, and TGFB1* (**Fig. 3d** and **Extended Data Fig. 2a**). WNT was upregulated across all subtypes, while other pathways showed subpopulation-specific expression patterns (**Fig. 3e**). Canonical Wnt signaling has been implicated in preserving ASPC proliferative capacity and inhibiting adipogenesis[34], and was also upregulated in most ASPC subpopulations in lymphedema. The coexistence of both pro-adipogenic and anti-adipogenic proliferation signatures across ASPC subpopulations may reflect the demand to continuously replenish adipocyte progenitor cells in the face of chronically dysregulated adipocyte hyperplasia. IGF2 protein concentration increases in lymphedema fluid[35] and induces differentiation of subcutaneous preadipocytes[36]; the IGF pathway was most strongly upregulated in ASPC^{CD81} and ASPC^{CD55}. CellChat[37] ligand-receptor modeling predicted increased IGF signaling to ASPCs originating from macrophages, lymphatic endothelial cells (LECs), and adipocytes in lymphedema (**Fig. 3f**). BMP-2 can enhance adipogenesis[38], and BMP signaling was upregulated in ASPC^{NAMPT} and ASPC^{CD81}, with a predicted blood endothelial cell (BEC) source (**Fig. 3g**). TGF-β1, which inhibits adipocyte differentiation but promotes collagen formation in models of lymphedema[39], was induced in anti-adipogenic ASPC^{PTCH2} and ASPC^{NAMPT}, which also express *COL271A1* and *COL4A4* (**Extended Data Fig. 2b**). Altogether, these data indicate that the ASPC response to lymphatic insufficiency is diverse and mediated by multiple distinct subpopulations.

A unique GRIA1^{+} population of ASPCs expands dramatically in lymphedema and expresses critical lymphangiogenic ligands

As part of our effort to link specific cell populations in the adipose niche to the pathology of lymphedema, we asked which cell types express genes that have been shown to cause primary lymphedema when mutated. As expected, most such genes show high or even dominant expression in LECs. We were surprised to note, however, that two lymphedema genes, *CCBE1* and *ADAMTS3*, are almost exclusively expressed by ASPCs (**Fig. 4a**). *CCBE1* and *ADAMTS3* encode components of the proteolytic cleavage machinery that activates VEGF-C to promote lymphangiogenesis[40–42], and when mutated, cause Hennekam lymphangiectasia–lymphedema syndrome[43,44]. In lymphedema subjects, ASPC *VEGFC* expression is positively correlated with fat deposition (**Fig. 4b**), and *VEGFC*, *ADAMTS3*, and *CCBE1* are co-expressed by the $ASPC^{GRIA1}$ population (**Fig. 4c-d**), which expands from 5.8% to 24.4% of total ASPCs ($p < 0.001$) (**Fig. 4e**). Accordingly, CellChat predicted increased VEGF network communication from ASPCs to LECs (**Fig. 4f**). $ASPC^{GRIA1}$ also specifically expresses additional secreted ligands which have been demonstrated to have pro-lymphangiogenic activity, including *SVEP1*[45,46] and *PDGFD*[47] (**Extended Data Fig. 3a**), and the proportion of $ASPC^{GRIA1}$ was positively associated with both fat and fluid areas by MRI (**Fig. 4g**). Interestingly, within lymphedema limb samples, $ASPC^{GRIA1}$ proportion was inversely correlated with severity of lymphedema as measured by perometry and trended toward a negative association with fluid area by MRI. $ASPC^{GRIA1}$ proportion had no association with fat area (**Extended Data Fig. 3b**), and was positively correlated with the proportion of LEC^{Cap}, but not LEC^{Col} (**Extended Data Fig. 3c**). *GRIA1* expression itself closely mirrors that of *VEGFC* (**Extended Data Fig. 3d-e**), making it a useful surface marker, and lymphedema-specific GRIA1 protein expression on ASPCs was confirmed with flow cytometry (**Fig. 4g** and **Extended Data Fig. 3f**). In lymphedema biopsy samples, $GRIA1^{+}PDGFRA^{+}$ stromal cells were found adjacent to $LYVE1^{+}$ lymphatic capillaries (**Fig. 4h**). In zebrafish, a population of fibroblasts co-express *vegfc, adamts3*, and *ccbe1* in proximity to lymphatic precursors during development[48], suggesting that this stromal pro-lymphatic program is highly conserved and essential for active lymphangiogenesis.

Lymphedema SAT exhibits active lymphangiogenesis

BECs and LECs were both significantly increased in lymphedema (**Fig. 1h**). Subclustering these populations revealed similar endothelial subpopulations to those previously described[12] (**Fig. 5a and Extended Data Fig. 4a**), including lymphatic capillary (LEC^{Cap}) and collecting duct (LEC^{Col}) populations, which were delineated with recently described markers of skin lymphatics[49] (**Fig. 5b**). Of these subpopulations, only LEC^{Cap} was significantly enriched as a proportion of total endothelial cells in lymphedema (**Fig. 5c** and **Extended Data Fig. 4b**). Subpopulations BECC2, one of two *ACKRA1*+ venous capillary populations[50], and LEC^{Col} demonstrated the highest angiogenesis scores calculated (**Fig. 5d**). The overall angiogenesis score was higher in lymphedema for both BECs and LECs (**Fig. 5e**).

A switch in signaling pathways was particularly evident in lymphatic capillaries, as FOXO and Notch were induced, and angiopoietin, Wnt, TGF-β, BMP, and IGF pathways were relatively downregulated (**Fig. 5f**). While FOXO1 is critical for developmental lymphangiogenesis[51], Notch1 quiescence is required for lymphatic development[52], but its activation has been shown to be essential in performing postnatal pathologic lymphangiogenesis[53]. TGF-β1[54] and BMPs, such as BMP-9[55], are anti-lymphangiogenic, while IGF[56], Wnt[57], and angiopoietin[58] typically play pro-lymphangiogenic roles, suggesting a complex balance of lymphatic remodeling is at work in lymphedema, particularly considering lymphatic collectors demonstrate upregulation of these pathways.

SAT biopsy sections stained for CD31 revealed foci of increased blood vascularization in lymphedema (**Extended Data Fig. 4c**). Labeling for LYVE1 and CD31 co-expression also confirmed the presence of lymphatic vessels within SAT (**Fig. 5g-h**). Quantification of paired biopsy sections demonstrated an increase in the number, average length, and total lymphatic length in lymphedema SAT (**Fig. 5i**), consistent with our sequencing data as well as prior literature[30]. Whether functional lymphatic vessels are being formed, however, remains unclear.

Lymphedema ASPC-secreted factors promote lymphatic endothelial tube elongation

Given the presence of a lymphedema-selective ASPC subpopulation that expresses pro-lymphatic secreted ligands in the setting of increased lymphatic vascularization, we sought to determine if ASPCs isolated from lymphedema patients exert a cell-autonomous pro-lymphangiogenic effect. We performed a matrigel tube formation assay using primary human dermal lymphatic endothelial cells (HDLECs) treated with culture media conditioned by ASPCs isolated from either unaffected control or lymphedema SAT (**Fig. 6a-b**). Treatment of HDLECs with lymphedema ASPC-conditioned media resulted in fewer, longer endothelial tubes (**Fig. 6c**). Conditioned media treatment of human umbilical vein endothelial cells (HUVECs), however, had no impact on any tube formation parameters (**Extended Data Fig. 5a**), suggesting a lymphatic-specific effect. Additionally, sorting GRIA1^{+} ASPCs from lymphedema SAT resulted in increased tube length compared to GRIA1^{-} ASPCs from the same subject (**Fig. 6d-e** and **Extended Data Fig. 5b**), suggesting that the principal pro-lymphatic effect is originating in ASPC^{GRIA1}.

HDLECs express *VEGFR3*, the primary receptor for VEGF-C, as compared to blood endothelial cells such as HUVECs, which express higher levels of *VEGFR2* (**Extended Data Fig. 5c**). Although VEGF-C can also induce signaling via VEGFR-2[59], when fully processed by CCBE1 the effect of VEGF-C on LECs is significantly more potent than on blood angiogenesis[60]. Treatment of HDLECs with recombinant human VEGF-C results in fewer, longer tubes in a tube formation assay (**Extended Data Fig. 5d**), consistent with the lymphatic response to lymphedema ASPC-conditioned media treatment. Although ELISAs for VEGF-C did not reveal a difference in total VEGF-C concentration in lymphedema or GRIA1+-conditioned media (**Extended Data Fig. 5e**), VEGF-C secreted by GRIA1+ ASPCs was more highly-processed than that secreted by GRIA1- ASPCs, indicated by a higher proportion of the 29/30 kD isoform of VEGF-C (**Fig. 6f-g**), which is associated with higher activity toward VEGFR-3[59]. Together with the sNuc-seq analysis, these data indicate that ASPCs upregulate *VEGFC* and its processing apparatus, including *CCBE1* (**Fig. 4c-d)**, to augment lymphangiogenesis in response to lymphatic insufficiency.

Discussion

Lymphedema is a complex, highly prevalent disease with a poorly-understood pathophysiology defined by both lymphatic dysfunction and dysregulated adipocyte differentiation. Due to challenges in modeling chronic lymphedema in animals, detailed characterization of affected human tissue is essential to developing insights into the underlying mechanisms of disease. In this study, we performed single-nucleus RNA sequencing on lymphedema-associated SAT and identified disease-specific cell states that are associated with adipocyte differentiation and lymphangiogenesis.

In lymphedema, a population of adipocytes expressing *SAA1* and *SAA2* becomes dramatically expanded, a phenomenon also observed in obesity-related adipose deposition[15,61]. However, while SAA expression is correlated with larger adipocyte size in obesity, we found lymphedema-associated adipocytes to be smaller than in control tissue, indicating that adipocyte hyperplasia, as opposed to hypertrophy, is the dominant mechanism of adipose expansion in lymphedema. Consistent with this paradigm, ASPCs isolated from lymphedema and unaffected SAT demonstrated an augmented propensity to undergo adipocyte differentiation *in vitro*, suggesting they have been primed for adipogenesis. To compensate for chronically disinhibited differentiation, the most stem-like ASPCs, including the $DPP4^{+}$ $ASPC^{CD55}$ population, upregulate genes associated with proliferation and Wnt signaling to maintain the adipocyte precursor pool. Our models of intracellular interactions and downstream signaling suggest that ASPCs may be targeted by IGF-2 and BMP-2 to potentiate these effects.

We also characterized the expansion of the lymphatic vasculature, particularly capillaries, in lymphedema. While bulk RNA sequencing of whole adipose tissue has demonstrated upregulated expression of *PDPN*, *FLT4* (VEGFR-3), and *VEGFC* in lymphedema[24,62,63], suggesting a pro-lymphangiogenic environment, the source of the factors regulating this process had not yet been identified. In this study, we have defined a previously undescribed lymphedema-associated *GRIA1*$^{+}$

ASPC population that physically associates with LECs *in vivo* and expresses the master lymphangiogenic factor *VEGFC*, its processing machinery, and other secreted agents with known pro-lymphatic actions. Culture media conditioned with both unsorted lymphedema ASPCs and GRIA1+ sorted ASPCs contained more mature VEGF-C and promoted LEC tube elongation in an *in vitro* model, indicating that lymphedema-associated ASPCs are programmed to promote lymphangiogenesis.

It is difficult to identify a single regulator of $ASPC^{GRIA1}$ activity, as our analysis indicates the role of multiple pathways. We found that TGFβ signaling genes are induced in lymphedema ASPC populations, and TGFβ-1 treatment is known to stimulate *VEGFC* expression in multiple cell types[64,65]. Wnt signaling is also upregulated in $ASPC^{GRIA1}$; Wnt signaling was required for *vegfc* expression in a zebrafish model of lymphangiogenesis[66], and a study of human medulloblastoma found higher *VEGFC* expression in tumors with aberrant activation of the Wnt pathway compared to other subtypes[67]. Exposure to VEGF-C itself has also been demonstrated to induce ASPC *VEGFC* expression and release[68], and may promote additional pro-lymphangiogenic mechanisms, such as secretion of exosomal microRNAs[69].

There has been interest in using ASPCs therapeutically for the treatment of secondary lymphedema[71], and the capacity of ASPCs to secrete lymphangiogenic factors, including VEGF-C, has been described in non-pathogenic settings[70]. Small trials of autologous ASPC transfer in humans with lymphedema, however, have thus far failed to show benefit with respect to limb volume or lymphoscintigraphic measures[72,73]. In our study population, lymphedema limb volume by perometry was reduced with increased prevalence of $ASPC^{GRIA1}$, but not other ASPC subpopulations, suggesting that the potential effectiveness of ASPCs to mitigate lymphedema, particularly the fluid component, may rely on being activated toward a pro-lymphangiogenic state. Further characterization of the upstream signaling that regulates this specialized ASPC identity should be the focus of future investigation.

In summary, this atlas provides a valuable resource to thoroughly interrogate the cell populations and activities that define secondary lymphedema in order to design mechanistic studies with the ultimate goal of developing clinically useful therapies and diagnostic biomarkers. Limitations of this study include limited sample size and lack of power to directly compare lymphedema etiologies, effect of subject sex, or limb affected. Subjects were recruited from a single center, and all samples used for sNuc-seq were obtained from Caucasian, non-Hispanic individuals.

Online methods

Subject enrollment and adipose tissue sample collection

All adult subjects with unilateral, fat-predominant (stage 2 or higher) lymphedema undergoing surgical debulking at BIDMC with a BMI between 18 and 35 kg/m^2 were screened for inclusion in this study, and were excluded for presence of the following: history of diabetes mellitus or use of glucose-lowering or weight loss medications; use of anti-estrogen agents, glucocorticoids, immunosuppression, or chemotherapy within the past 6 months; history of HIV/AIDS; or active malignancy. Subjects provided written informed consent preoperatively and were not compensated for their participation (BIDMC IRB 2021P000364). Subcutaneous adipose tissue for sequencing, approximately 50 mg, was resected en bloc at the start of the surgical case under general anesthesia via a 4 mm incision and snap frozen immediately in liquid nitrogen. Biopsies for histological slide preparation were obtained using a 6 mm biopsy punch (Fisher Scientific) and placed on ice. Lipoaspirate, approximately 20 mL, was obtained as per standard of care at the beginning of the case using power assisted liposuction as described elsewhere[74].

Single-nucleus RNA sequencing and data analysis

SAT sNuc-seq was performed as previously described[75]. Briefly, adipose samples were homogenized in TST buffer using a gentleMACS Dissociator (Miltenyi Biotec). Lysate was filtered through 40 µm and 20 µm nylon filters (CellTreat) and washed. After the second wash, each sample was incubated with

NucBlue (Thermofisher Scientific) as well as an individual hashtag antibody (BioLegend) for 45 minutes. After incubation, nuclei were washed and flow sorted together into RT Reagent B (10x Genomics) using a Beckman Coulter MoFlo Astrios EQ with a 70 µm nozzle. After sorting, samples were immediately loaded on the 10x Chromium controller (10x Genomics) according to the manufacturer's protocol. Single Cell 3' v3.1 chemistry was used to process all samples and cDNA and gene expression libraries were generated according to the manufacturer's instructions (10x Genomics). Gene expression libraries were multiplexed and sequenced on the Nextseq 500 (Illumina).

Raw sequencing reads were processed into digital expression matrices (DGE) using CellRanger (10x Genomics, version 6.1.2) and using annotation GENCODE-v44. DemuxEM32 (version 0.1.6) was used to sort cells into individual samples based on their antibody hashtags. Ambient RNA was removed from the processed DGEs using CellBender (version 0.2.0), and doublet scores were calculated using both scDblFinder(version 1.2.0) and scds (version 1.4.0). Cells were removed as doublets if they were both determined to be a doublet using scDblFinder and if they had a scds hybrid score > 1.5. Cells with < 800 UMIs were removed from the dataset, as were cells with > 10% of mitochondrial reads. Genes found in fewer than 2 cells were removed. The data were then normalized using SCTransform and integrated using RPCA in Seurat (version 4.1.1), integrating by individual. To subcluster, cells were subset into broad cell types and reintegrated and clusters were recalculated. Subclusters with high doublet scores and/or high percentages of mitochondrial reads were removed and the data was again reintegrated and clusters were recalculated.

Reference mapping was performed between the reported dataset and the human subcutaneous dataset from Emont et. al. (2022) using Seurat multimodal reference mapping. To annotate cell types, calculated clusters were evaluated for similarity to previously annotated clusters. If clusters mapped exactly, they were annotated as the same cell type. If not, they were evaluated for distinct marker genes

and annotated as a new cluster. All clusters without distinct names were renamed to be defined by a top marker gene.

To calculate pseudobulk counts, objects for individual cell types were split by sample and randomly subset to contain the same number of cells per sample. Differential expression analysis (DEA) was run on pseudobulk samples using edgeR (version 3.30.3). To reduce the variation introduced by the random subsampling, subsampling and DEA were performed 10,000 times; significantly regulated genes used on plots and for correlation analysis were defined as those with log2 fold change greater than 0.5 and FDR less than 0.1 in at least 9,000 iterations. To plot, heatmaps were generated using pseudobulk sums of all cells in each sample, and edgeR was used to calculate cpms from the pseudobulk counts. PCA plots were generated using a randomly subsampled pseudobulk dataset. Heatmaps were plotted using pheatmap (version 1.0.12).

Predicted intercellular interactions and downstream signaling pathways were determined using NicheNet[33] and CellChat[37]. Signature scores were calculated using Vision 3.0.0[76] using gene lists from the Molecular Signatures Database[19] as listed in **Supplementary Table 3**. Comparisons between groups were performed using a Wilcoxon rank sum test.

MRI imaging analysis

ImageJ was used to manually segment and threshold fat on fat-weighted MR sequences of the bilateral extremities at the approximate level of the biopsies in order to calculate fat volume, fluid volume, fat fraction and total subcutaneous area in the affected and unaffected contralateral extremity.

Histology and immunofluorescent labeling

Tissue biopsies were immediately placed on ice, washed with PBS, and fixed in 10% formalin overnight at 4°C, followed by paraffin embedding, sectioning, and staining with hematoxylin and eosin (H&E). Unstained sections for immunofluorescence were deparaffinized and rehydrated by heating to 55°C

and sequential washing in xylene, 100%, 95%, 70%, 50% ethanol and deionized water. Antigen retrieval was performed in sub-boiling 10 mM sodium citrate buffer (pH 6.0) for 10 min. Sections were washed with 1% donkey serum in PBS with 0.4% Triton X-100 (PBS-T) twice and blocked with 5% donkey serum in PBS-T for 30 minutes. Sections were then incubated with the primary antibodies diluted in 1% donkey serum PBS-T at room temperature for 1 h and then at 4°C overnight. Primary antibody and dilutions used for labeling were: Alexa Fluor 488 rabbit anti-PLIN1 (1:100, Cell Signaling, 29138S), goat anti-LYVE 1 (1:100, R&D Systems, AF2089), rabbit anti-CD31 (1:200, Proteintech, 11265-1-AP), and FITC GRIA1 (1:50, Thermo Scientific, MA45628). Samples were subsequently incubated with secondary antibodies diluted in PBS-T at room temperature for 1 hour. Secondary antibodies used were: Alexa Fluor 647 donkey anti-goat (1:250, Thermo Scientific, A-31571), Alexa Fluor 568 donkey anti-mouse (1:250, Thermo Scientific, A-19937), Alexa Fluor 568 donkey anti-rabbit (1:250, Thermo Scientific, A-10042) and Hoechst 33342 (1:1000, Invitrogen, H3570). Images were obtained using a fluorescent slide scanner and Zeiss LSM 880 laser scanning confocal system running Zen Black 2.3 software.

Adipocyte size and lymphatic vessel quantification

To measure adipocyte size, H&E and confocal BODIPY-labeled images were analyzed using Adiposoft v1.16[77] in ImageJ Fiji. All counts were manually verified, and adipocytes inaccurately delineated in automatic mode were manually adjusted. Lymphatic vessels were measured using ImageJ Fiji software. Vascular structures double-labeled for LYVE1 and CD31 were measured length-wise, or for vessels cut in cross-section, measurement was done along the longest axis.

TCA precipitation, Western blotting, and ELISA

100 µL of 100% trichloroacetic acid was added per 1 mL of GRIA1+ or GRIA1- ASPC conditioned media. Samples were vortexed, incubated on ice for one hour, and centrifuged for ten minutes at 10,000 x g. The supernatant was aspirated and the pellet washed with ice cold acetone. After allowing the

pellet to air dry, precipitated protein was resuspended in 50 µL 2X Laemmli sample buffer (Bio-Rad). Protein samples were separated by SDS-PAGE, transferred to polyvinylidene difluoride (PVDF) membranes (Bio-Rad), and incubated with primary antibodies: mouse-anti VEGF-C (detected 29/30 kD isoform, 1:200, Santa Cruz, sc-53462), rabbit-anti VEGF-C (detected 43 kD isoform, 1:1000, Proteintech, 22601-1-AP); followed by HRP-conjugated secondary antibodies: donkey-anti rabbit IgG (1:10,000, Fisher Scientific 45-000-682), sheep-anti mouse IgG (1:10,000, Fisher Scientific 45-000-679). VEGF-C ELISA was performed on non-precipitated ASPC-conditioned media samples using human VEGFC ELISA kit (Abcam, 100664).

Cell culture and flow cytometry

Fresh lipoaspirate was incubated with collagenase type II (1 mg/ml) (Sigma-Aldrich) in digestion buffer (Hanks' balanced salt solution with calcium and magnesium supplemented with 0.5% bovine serum albumin) on a shaker water bath incubator at 37°C for 20 minutes with vigorous shaking by hand every 5 minutes. EDTA, pH 8.0 at a concentration of 10 mM was then added for an additional 5 minutes, after which wash media (DMEM+glutamax with 10% fetal bovine serum (FBS) and 1% penicillin-streptomycin) or FACS buffer (PBS with 1mM EDTA, 25 mM HEPES and 1% FBS) was added. Cells were filtered through a 100 µm filter and washed, and if flow cytometry was to be performed, incubated with ACK lysis buffer for 5 minutes. SVF was then washed and filtered through 40 µm filter followed by plating on multiwell plates in growth media (DMEM+glutamax, 15% FBS, 1% penicillin-streptomycin) or suspended in FACS buffer for flow cytometry. Human primary dermal lymphatic endothelial cells (HDLEC, Cell Biologics, H-6064) and human umbilical vein endothelial cells (HUVEC, gift from Shingo Kajimura) were maintained on gelatin-coated flasks in complete human endothelial cell media (Cell Biologics, H-1168).

For flow cytometry, cells were incubated with the appropriate antibody for 45 minutes at room temperature followed by two washes. Antibodies used for flow cytometry included: FITC GRIA1

(Thermo Scientific, MA45628), Brilliant Violet 421 mouse anti-human CD31 (BioLegend, 303123), and Brilliant Violet 421 mouse anti-human CD45 (BioLegend, 368521) Flow cytometric cell sorting and analysis was performed on a SORP FACSAria III (BD) and data was processed using FlowJo version 10.7.1 (BD).

To determine adipogenic potential, ASPCs (passage 3-5) were cultured in growth media until confluence, followed by 3 days in differentiation induction media (DMEM+glutamax, 10% FBS, 1% penicillin-streptomycin, 0.5 µg/ml insulin, 5 µM dexamethasone, 5 µM rosiglitazone, and 0.5 mM 3-isobutyl-1-methylxanthine, 33 µM biotin, and 17 µM pantothenic acid), followed by 7 days in maintenance media (induction media without IBMX or rosiglitazone), with media change every 2-3 days. Cells were imaged, then washed and lysed in Trizol for RNA purification and qPCR.

RT-quantitative PCR

Cells were collected in Trizol as described above. Total RNA was isolated using the E.Z.N.A. Total RNA Kit II (Omega Bio-Tek) per manufacturer's instructions. RNA concentration was quantified using NanoDrop One (Thermo Scientific) and up to 1 µg of RNA was reverse-transcribed using High-Capacity cDNA Reverse Transcription Kit (Thermo Fisher). SYBR Green PCR Master Mix (Thermo Fisher) and gene primers (**Supplementary Table 4**) were used to perform RT-qPCR using QuantStudio 6 Flex Real-time PCR system. Expression was normalized to the housekeeping gene *ACTB*. Results are presented as fold change ($2^{-\Delta CT}$).

Conditioned media (CM) generation and* in vitro *tube formation assays

ASPCs at passages 3-5 were grown to confluence in 6 well plates. DMEM+glutamax supplemented with 0.5% FBS and 1% pen-strep, 2 mL per well, was conditioned at 37°C for 48 hours, centrifuged at 10,000 G for 10 minutes at 4°C to remove cellular debris, and stored at -80°C. To perform tube formation assays, growth-factor reduced Matrigel (Corning) was added to 96 well plates, followed by addition of 1.5 x 10^4 HDLECs or HUVECs per well in complete EC media. Imaging was performed at

18 hours after plating, and tube networks were analyzed using Angiogenesis Analyzer for ImageJ[78]. For CM experiments, CM was mixed 1:1 with complete EC media at the time of cell plating. Recombinant human VEGF-C (BioLegend, 589702) was used at a concentration of 50 ng/mL.

Data availability

Raw and processed sNuc-seq data will be available on GEO at the time of publication. Data from the Emont et. al. 2022 study is publicly available: GSE176067.

References

1. Grada, A. A. & Phillips, T. J. Lymphedema: Pathophysiology and clinical manifestations. *J Am Acad Dermatol* **77**, 1009–1020 (2017).

2. Kurt, H. *et al.* Massive localized lymphedema: a clinicopathologic study of 46 patients with an enrichment for multiplicity. *Modern Pathology* **29**, 75–82 (2016).

3. Jäger, G., Döller, W. & Roth, R. Quality-of-life and body image impairments in patients with lymphedema. *Lymphology* **39**, 193–200 (2006).

4. Rockson, S. G., Keeley, V., Kilbreath, S., Szuba, A. & Towers, A. Cancer-associated secondary lymphoedema. *Nat Rev Dis Primers* **5**, 22 (2019).

5. DiSipio, T., Rye, S., Newman, B. & Hayes, S. Incidence of unilateral arm lymphoedema after breast cancer: a systematic review and meta-analysis. *Lancet Oncol* **14**, 500–515 (2013).

6. Greene, A. K. Epidemiology and Morbidity of Lymphedema. in *Lymphedema: Presentation, Diagnosis, and Treatment* (eds. Greene, A. K., Slavin, S. A. & Brorson, H.) 33–44 (Springer International Publishing, Cham, 2015). doi:10.1007/978-3-319-14493-1_4.

7. Greene, A. K. & Sudduth, C. L. Lower extremity lymphatic function predicted by body mass index: a lymphoscintigraphic study of obesity and lipedema. *Int J Obes* **45**, 369–373 (2021).

8. Rannikko, E. H. *et al.* Phase II study shows potential benefit of adenoviral vascular endothelial growth factor C (VEGF-C) and lymph node transfer in lymphedema. *Plastic and Reconstructive Surgery* 10.1097/PRS.0000000000011675 (2021) doi:10.1097/PRS.0000000000011675.

9. Rockson, S. G. *et al.* Pilot studies demonstrate the potential benefits of antiinflammatory therapy in human lymphedema. *JCI Insight* **3**, (2018).

10. Westcott, G. P. & Rosen, E. D. Crosstalk Between Adipose and Lymphatics in Health and Disease. *Endocrinology* **163**, (2022).

11. Escobedo, N. & Oliver, G. The lymphatic vasculature: its role in adipose metabolism and obesity. *Cell Metab* **26**, 598–609 (2017).

12. Emont, M. P. *et al.* A single-cell atlas of human and mouse white adipose tissue. *Nature* **603**, 926–933 (2022).

13. Alsharif, H. *et al.* Loss of Brain Angiogenesis Inhibitor-3 (BAI3) G-Protein Coupled Receptor in Mice Regulates Adaptive Thermogenesis by Enhancing Energy Expenditure. *Metabolites* **13**, 711 (2023).

14. Yuan, F. *et al.* Spermidine/spermine N1-acetyltransferase-mediated polyamine catabolism regulates beige adipocyte biogenesis. *Metabolism* **85**, 298–304 (2018).

15. Poitou, C. *et al.* Serum amyloid A: production by human white adipocyte and regulation by obesity and nutrition. *Diabetologia* **48**, 519–528 (2005).

16. Qu, R. *et al.* The role of serum amyloid A1 in the adipogenic differentiation of human adipose-derived stem cells basing on single-cell RNA sequencing analysis. *Stem Cell Research & Therapy* **13**, 187 (2022).

17. Poitou, C. *et al.* Role of serum amyloid a in adipocyte-macrophage cross talk and adipocyte cholesterol efflux. *J Clin Endocrinol Metab* **94**, 1810–1817 (2009).

18. Sjöholm, K., Lundgren, M., Olsson, M. & Eriksson, J. W. Association of serum amyloid A levels with adipocyte size and serum levels of adipokines: Differences between men and women. *Cytokine* **48**, 260–266 (2009).

19. Liberzon, A. *et al.* The Molecular Signatures Database (MSigDB) hallmark gene set collection. *Cell Syst* **1**, 417–425 (2015).

20. Gupta, A. *et al.* Mapping the transcriptional landscape of human white and brown adipogenesis using single-nuclei RNA-seq. *Mol Metab* **74**, 101746 (2023).

21. Zhang, J., Hoffner, M. & Brorson, H. Adipocytes are larger in lymphedematous extremities than in controls. *J Plast Surg Hand Surg* 1–8 (2021) doi:10.1080/2000656X.2021.1953042.

22. von Atzigen, J. *et al.* A Comparative Analysis to Dissect the Histological and Molecular Differences among Lipedema, Lipohypertrophy and Secondary Lymphedema. *International Journal of Molecular Sciences* **24**, 7591 (2023).

23. Wolf, S. *et al.* Is Lymphedema a Systemic Disease? A Paired Molecular and Histological Analysis of the Affected and Unaffected Tissue in Lymphedema Patients. *Biomolecules* **12**, 1667 (2022).

24. Koc, M. *et al.* Lymphedema alters lipolytic, lipogenic, immune and angiogenic properties of adipose tissue: a hypothesis-generating study in breast cancer survivors. *Sci Rep* **11**, 8171 (2021).

25. Stromsdorfer, K. L. *et al.* NAMPT-Mediated NAD+ Biosynthesis in Adipocytes Regulates Adipose Tissue Function and Multi-organ Insulin Sensitivity in Mice. *Cell Reports* **16**, 1851–1860 (2016).

26. Nielsen, K. N. *et al.* NAMPT-mediated NAD+ biosynthesis is indispensable for adipose tissue plasticity and development of obesity. *Molecular Metabolism* **11**, 178 (2018).

27. Qi, N. *et al.* Adipocyte-specific inactivation of NAMPT, a key NAD+ biosynthetic enzyme, causes a metabolically unhealthy lean phenotype in female mice during aging. *American Journal of Physiology-Endocrinology and Metabolism* **327**, E81–E88 (2024).

28. Oguri, Y. *et al.* CD81 Controls Beige Fat Progenitor Cell Growth and Energy Balance via FAK Signaling. *Cell* **182**, 563-577.e20 (2020).

29. Merrick, D. *et al.* Identification of a mesenchymal progenitor cell hierarchy in adipose tissue. *Science* **364**, eaav2501 (2019).

30. Schwalie, P. C. *et al.* A stromal cell population that inhibits adipogenesis in mammalian fat depots. *Nature* **559**, 103–108 (2018).

31. Levi, B. *et al.* Molecular analysis and differentiation capacity of adipose-derived stem cells from lymphedema tissue. *Plast Reconstr Surg* **132**, 580–589 (2013).

32. Xiang, Q. *et al.* Transcriptome analysis and functional identification of adipose-derived mesenchymal stem cells in secondary lymphedema. *Gland Surg* **9**, 558–574 (2020).

33. Browaeys, R., Saelens, W. & Saeys, Y. NicheNet: modeling intercellular communication by linking ligands to target genes. *Nat Methods* **17**, 159–162 (2020).

34. Yang Loureiro, Z. *et al.* Wnt signaling preserves progenitor cell multipotency during adipose tissue development. *Nat Metab* **5**, 1014–1028 (2023).

35. Hsiao, H.-Y., Liu, J.-W., Pappalardo, M. & Cheng, M.-H. The Impacts of Lymph on the Adipogenesis of Adipose-Derived Stem Cells. *Plastic and Reconstructive Surgery* **151**, 1005 (2023).

36. Alfares, M. N., Perks, C. M., Hamilton-Shield, J. P. & Holly, J. M. P. Insulin-like growth factor-II in adipocyte regulation: depot-specific actions suggest a potential role limiting excess visceral adiposity. *Am J Physiol Endocrinol Metab* **315**, E1098–E1107 (2018).

37. Jin, S. *et al.* Inference and analysis of cell-cell communication using CellChat. *Nat Commun* **12**, 1088 (2021).

38. Denton, N. F. *et al.* Bone morphogenetic protein 2 is a depot-specific regulator of human adipogenesis. *Int J Obes* **43**, 2458–2468 (2019).

39. Baik, J. E. *et al.* TGF-β1 mediates pathologic changes of secondary lymphedema by promoting fibrosis and inflammation. *Clin Transl Med* **12**, e758 (2022).

40. Jeltsch, M. *et al.* CCBE1 enhances lymphangiogenesis via A disintegrin and metalloprotease with thrombospondin motifs-3-mediated vascular endothelial growth factor-C activation. *Circulation* **129**, 1962–1971 (2014).

41. Jha, S. K. *et al.* Efficient activation of the lymphangiogenic growth factor VEGF-C requires the C-terminal domain of VEGF-C and the N-terminal domain of CCBE1. *Sci Rep* **7**, 4916 (2017).

42. Bui, H. M. *et al.* Proteolytic activation defines distinct lymphangiogenic mechanisms for VEGFC and VEGFD. *J Clin Invest* **126**, 2167–2180 (2016).

43. Alders, M. *et al.* Mutations in CCBE1 cause generalized lymph vessel dysplasia in humans. *Nat Genet* **41**, 1272–1274 (2009).

44. Brouillard, P. *et al.* Loss of ADAMTS3 activity causes Hennekam lymphangiectasia-lymphedema syndrome 3. *Hum Mol Genet* **26**, 4095–4104 (2017).

45. Michelini, S. *et al.* SVEP1 is important for morphogenesis of lymphatic system: Possible implications in lymphedema. *Lymphology* **54**, 12–22 (2021).

46. Hußmann, M. *et al.* Svep1 is a binding ligand of Tie1 and affects specific aspects of facial lymphatic development in a Vegfc-independent manner. *eLife* **12**, e82969 (2023).

47. Cadamuro, M. *et al.* Platelet-derived growth factor-D enables liver myofibroblasts to promote tumor lymphangiogenesis in cholangiocarcinoma. *J Hepatol* **70**, 700–709 (2019).

48. Wang, G. *et al.* Specific fibroblast subpopulations and neuronal structures provide local sources of Vegfc-processing components during zebrafish lymphangiogenesis. *Nat Commun* **11**, 2724 (2020).

49. Chovatiya, G., Li, K. N., Li, J., Ghuwalewala, S. & Tumbar, T. Alk1 acts in non-endothelial VE-cadherin+ perineurial cells to maintain nerve branching during hair homeostasis. *Nat Commun* **14**, 5623 (2023).

50. Thiriot, A. *et al.* Differential DARC/ACKR1 expression distinguishes venular from non-venular endothelial cells in murine tissues. *BMC Biology* **15**, 45 (2017).

51. Niimi, K. *et al.* FOXO1 regulates developmental lymphangiogenesis by upregulating CXCR4 in the mouse-tail dermis. *Development* **147**, dev181545 (2020).

52. Zheng, W. *et al.* Notch restricts lymphatic vessel sprouting induced by vascular endothelial growth factor. *Blood* **118**, 1154–1162 (2011).

53. Niessen, K. *et al.* The Notch1-Dll4 signaling pathway regulates mouse postnatal lymphatic development. *Blood* **118**, 1989–1997 (2011).

54. Clavin, N. W. *et al.* TGF-beta1 is a negative regulator of lymphatic regeneration during wound repair. *Am J Physiol Heart Circ Physiol* **295**, H2113-2127 (2008).

55. Yoshimatsu, Y. *et al.* Bone morphogenetic protein-9 inhibits lymphatic vessel formation via activin receptor-like kinase 1 during development and cancer progression. *Proceedings of the National Academy of Sciences* **110**, 18940–18945 (2013).

56. Björndahl, M. *et al.* Insulin-like growth factors 1 and 2 induce lymphangiogenesis in vivo. *Proc Natl Acad Sci U S A* **102**, 15593–15598 (2005).

57. Cha, B. *et al.* Mechanotransduction activates canonical Wnt/β-catenin signaling to promote lymphatic vascular patterning and the development of lymphatic and lymphovenous valves. *Genes Dev* **30**, 1454–1469 (2016).

58. Akwii, R. G. *et al.* Angiopoietin-2-induced lymphatic endothelial cell migration drives lymphangiogenesis via the β1 integrin-RhoA-formin axis. *Angiogenesis* **25**, 373–396 (2022).

59. Joukov, V. *et al.* Proteolytic processing regulates receptor specificity and activity of VEGF-C. *The EMBO Journal* **16**, 3898–3911 (1997).

60. Jeltsch, M. *et al.* Hyperplasia of lymphatic vessels in VEGF-C transgenic mice. *Science* **276**, 1423–1425 (1997).

61. Yang, R.-Z. *et al.* Acute-phase serum amyloid A: an inflammatory adipokine and potential link between obesity and its metabolic complications. *PLoS Med* **3**, e287 (2006).

62. Zamora, A. *et al.* 15-Lipoxygenase promotes resolution of inflammation in lymphedema by controlling Treg cell function through IFN-β. *Nat Commun* **15**, 221 (2024).

63. Karaman, S. *et al.* Multi-omics characterization of lymphedema-induced adipose tissue resulting from breast cancer-related surgery. *The FASEB Journal* **38**, e70097 (2024).

64. Suzuki, Y. *et al.* Transforming growth factor-β induces vascular endothelial growth factor-C expression leading to lymphangiogenesis in rat unilateral ureteral obstruction. *Kidney International* **81**, 865–879 (2012).

65. Pak, K. H., Park, K. C. & Cheong, J.-H. VEGF-C induced by TGF- β1 signaling in gastric cancer enhances tumor-induced lymphangiogenesis. *BMC Cancer* **19**, 799 (2019).

66. Gore, A. V. *et al.* Rspo1/Wnt signaling promotes angiogenesis via Vegfc/Vegfr3. *Development* **138**, 4875–4886 (2011).

67. Penco-Campillo, M. *et al.* VEGFC negatively regulates the growth and aggressiveness of medulloblastoma cells. *Commun Biol* **3**, 1–14 (2020).

68. Zhang, L. *et al.* ADSCs stimulated by VEGF-C alleviate intestinal inflammation via dual mechanisms of enhancing lymphatic drainage by a VEGF-C/VEGFR-3-dependent mechanism and inhibiting the NF-κB pathway by the secretome. *Stem Cell Res Ther* **13**, 448 (2022).

69. Wang, X., Wang, H., Cao, J. & Ye, C. Exosomes from Adipose-Derived Stem Cells Promotes VEGF-C-Dependent Lymphangiogenesis by Regulating miRNA-132/TGF-β Pathway. *Cellular Physiology and Biochemistry* **49**, 160–171 (2018).

70. Ahmadzadeh, N. *et al.* Human adipose-derived stem cells support lymphangiogenesis *in vitro* by secretion of lymphangiogenic factors. *Experimental Cell Research* **388**, 111816 (2020).

71. Lafuente, H., Jaunarena, I., Ansuategui, E., Lekuona, A. & Izeta, A. Cell therapy as a treatment of secondary lymphedema: a systematic review and meta-analysis. *Stem Cell Res Ther* **12**, 578 (2021).

72. Toyserkani, N. *et al.* Adipose-derived regenerative cells and fat grafting for treating breast cancer-related lymphedema: Lymphoscintigraphic evaluation with 1 year of follow-up. *Journal of Plastic, Reconstructive & Aesthetic Surgery* **72**, 71–77 (2019).

73. Jørgensen, M. G. *et al.* Adipose-derived regenerative cells and lipotransfer in alleviating breast cancer-related lymphedema: An open-label phase I trial with 4 years of follow-up. *Stem Cells Translational Medicine* **10**, 844–854 (2021).

74. Granoff, M. D., Pardo, J. & Singhal, D. Power-Assisted Liposuction: An Important Tool in the Surgical Management of Lymphedema Patients. *Lymphat Res Biol* **19**, 20–22 (2021).

75. Gulko, A. *et al.* Protocol for flow cytometry-assisted single-nucleus RNA sequencing of human and mouse adipose tissue with sample multiplexing. *STAR Protocols* **5**, 102893 (2024).

76. Jones, M., Detomaso, D., Ashuach, T. & Rosen, Y. VISION: Functional interpretation of single cell RNA-seq latent manifolds. (2022).

77. Galarraga, M. *et al.* Adiposoft: automated software for the analysis of white adipose tissue cellularity in histological sections. *Journal of Lipid Research* **53**, 2791–2796 (2012).

78. Carpentier, G. *et al.* Angiogenesis Analyzer for ImageJ — A comparative morphometric analysis of “Endothelial Tube Formation Assay” and “Fibrin Bead Assay”. *Scientific Reports* **10**, 11568 (2020).

Acknowledgements

We gratefully acknowledge the BIDMC Department of Surgery FIRST program for their help with developing and maintaining the IRB protocol for subject enrollment and sample collection, and the Boston Area Diabetes Endocrinology Research Center Functional Genomics and Bioinformatics Core (supported by RC2 DK116691) for performing sNuc-seq. GPW is supported by NIH K08 DK132413. EDR is supported by NIH R01 DK126789. MPE is supported by NIH K01 DK134806. TPP is supported by NIH R01 CA284372 and DoD HT94252410100.

Figure Legends

Figure 1. Single-nucleus RNA sequencing atlas of lymphedema-associated subcutaneous adipose tissue. *a,* Tissue collection sites; *b,* MRI data workflow; *c*, Quantification of MRI parameters **(Supplementary Table 2)**; *d*, Hematoxylin and eosin staining of control and lymphedema biopsies; *e*, Perilipin 1 immunofluorescence of control and lymphedema biopsies; *f*, UMAP of lymphedema sNuc-seq atlas, including 23,777 cells; *g*, Marker genes for cell clusters identified by sNuc-seq; *h*, Proportions of cell types per individual sample. ASPC, adipose stem and progenitor cell; BEC, blood endothelial cell; DC, dendritic cell; LEC, lymphatic endothelial cell; NK: natural killer; SC: subcutaneous; SMC: smooth muscle cell; *, $p<0.05$; **, $p<0.01$; ***, $p<0.001$

Figure 2. Lymphedema is characterized by expansion of *SAA*$^{+}$ adipocytes and enhanced ASPC adipogenic potential. Adipocyte (*a-c*) subpopulations, relative proportions, and marker genes; *d*, Adipogenesis and stem cell proliferation scores disaggregated by subpopulation and disease state; *e*, Adipogenesis score across all adipocytes; *f*, Hematoxylin and eosin staining of representative adipose samples; *g-h*, Adipocyte size quantification across paired samples from three subjects; ASPC (*i-k*) subpopulations, relative proportions, and marker genes; *l*, Adipogenesis score across all ASPCs; *m-n*, Light microscopy and qPCR of *ex vivo* differentiated ASPCs from a control and lymphedema subject. C, control; L, lymphedema; DMI, dexamethasone, IBMX, and insulin; TZD, thiazolidinedione; *, $p<0.05$; **, $p<0.01$; ***, $p<0.001$; ****, $p<0.0001$

Figure 3. Lymphedema-associated ASPCs upregulate a subset of genes that correlate with disease severity and demonstrate augmented WNT, IGF, and BMP signaling. *a*, Heatmap of significant genes from ASPC pseudobulk analysis by sample; *b*, Heatmap of Pearson correlations of pseudobulk genes and MRI imaging characteristics, and categorization of volume-associated genes; *c*, Positively correlated volume-associated gene expression by ASPC subpopulation; *d*, NicheNet

(sender-agnostic) modeling of ASPC receptor-mediated signaling pathways increased in lymphedema; *e*, Selected signaling signature scores by ASPC subpopulation; *f-g*, CellChat intercellular interaction modeling between cell types.

Figure 4. GRIA1$^+$ ASPCs expand dramatically in lymphedema and express essential lymphangiogenic ligands. *a*, Selected genes associated with primary lymphedema syndromes plotted against cell subpopulations; *b*, *VEGFC* expression correlation with fat volume by MRI; *c*, Violin plots of gene expression within ASPC subpopulations; *d*, Joint density plot of VEGF-C related genes; *e*, UMAP plot of ASPC^{GRIA1} population in control and lymphedema; *f*, CellChat plot of predicted VEGF network ligand-receptor interactions; *g*, Correlation of ASPC^{GRIA1} with MRI-derived fat and fluid areas; *h*, Flow cytometry for GRIA1$^+$ stromal cells; *i*, Immunofluorescence of lymphedema biopsy for GRIA1$^+$PDGFRA$^+$ stromal cells (closed arrowheads) and lymphatic capillaries (open arrowheads).

Figure 5. Lymphedema-associated SAT exhibits lymphangiogenesis. *a*, UMAP plots of endothelial populations split by disease status; *b*, Lymphatic capillary and collecting duct endothelial cell markers; *c*, LEC subpopulations as a proportion of total endothelial cells; *d*, Angiogenesis signature scores by subpopulation and *e*, across total BEC and LEC populations; *f*, Signaling pathway scores by endothelial subpopulation; *g*, Immunofluorescence of a representative lymphatic capillary and *h*, of a lower-power SAT field (arrow heads: LYVE1$^+$CD31$^+$ LVs); *i*, Quantification of lymphatic vessels by immunofluorescence of paired biopsies.

Figure 6. Lymphedema ASPC-secreted factors promote lymphatic endothelial tube elongation *ex vivo*. *a*, Experimental paradigm for conditioned media experiments; *b*, Representative light microscopy of Matrigel tube formation assays at 18 hours; *c*, HDLEC tube parameters at 18 hours of treatment; *d*, Experimental paradigm for sorted ASPC conditioned media experiments; *e*, HDLEC

tube parameters at 18 hours of treatment with sorted ASPC-conditioned media; *f*, Western blot of VEGF-C isoforms; *g*, Quantification of band intensity from Western blot. NCM, non-conditioned media; ns: Non-significant; *, p<0.05; **, p<0.01; ****, p<0.0001.

Extended Data Figure 1. *a,* Adipocyte label transfer to Emont, et. al. reference populations; *b*, Adipocyte subpopulation proportions; *c*, *SAA1* and *SAA2* expression violin plots across adipocyte subpopulations; *d*, Adipogenesis score disaggregated by individual and cell type; *e*, Quantification of adipocyte size on BODIPY-labeled SAT whole mount; *f,* ASPC label transfer to Emont, et. al. reference populations; *g*, ASPC subpopulation proportions. *, p<0.05; ***, p<0.001.

Extended Data Figure 2. *a,* NicheNet analysis (sender-focused) of ASPC ligand-receptor interactions; *b,* Selected collagen gene expression of $ASPC^{NAMPT}$.

Extended Data Figure 3. *a*, Dot plot of *SVEP1* and *PDGFD* expression; *b*, Proportion of $ASPC^{GRIA1}$ plotted against perometry measurements and MRI fluid and fat areas; *c*, Proportion of $ASPC^{GRIA1}$ (as a proportion of ASPCs) plotted against LEC subpopulations (as a proportion of all cells); *d*, *VEGFC* and *GRIA1* ASPC feature plots split by disease state; *e*, Scatter plot of *VEGFC* and *GRIA1* within ASPC populations; *f*, GRIA1 flow cytometry gating strategy.

Extended Data Figure 4. *a*, Selected marker genes for endothelial cell populations; *b*, BEC subpopulations as a proportion of total endothelial cells; *c*, Representative immunofluorescence for CD31 of paired SAT biopsies.

Extended Data Figure 5. *a*, HUVEC tube parameters at 18 hours of treatment; *b*, HDLEC tube parameters at 18 hours of treatment with sorted ASPC-conditioned media; *c*, qPCR for selected

endothelial identity genes; *d*, HDLEC tube parameters at 18 hours of treatment with recombinant human VEGF-C; *e*, VEGF-C ELISA of conditioned media. *, $p<0.05$; **, $p<0.01$; ***, $p<0.001$.

Figure 1

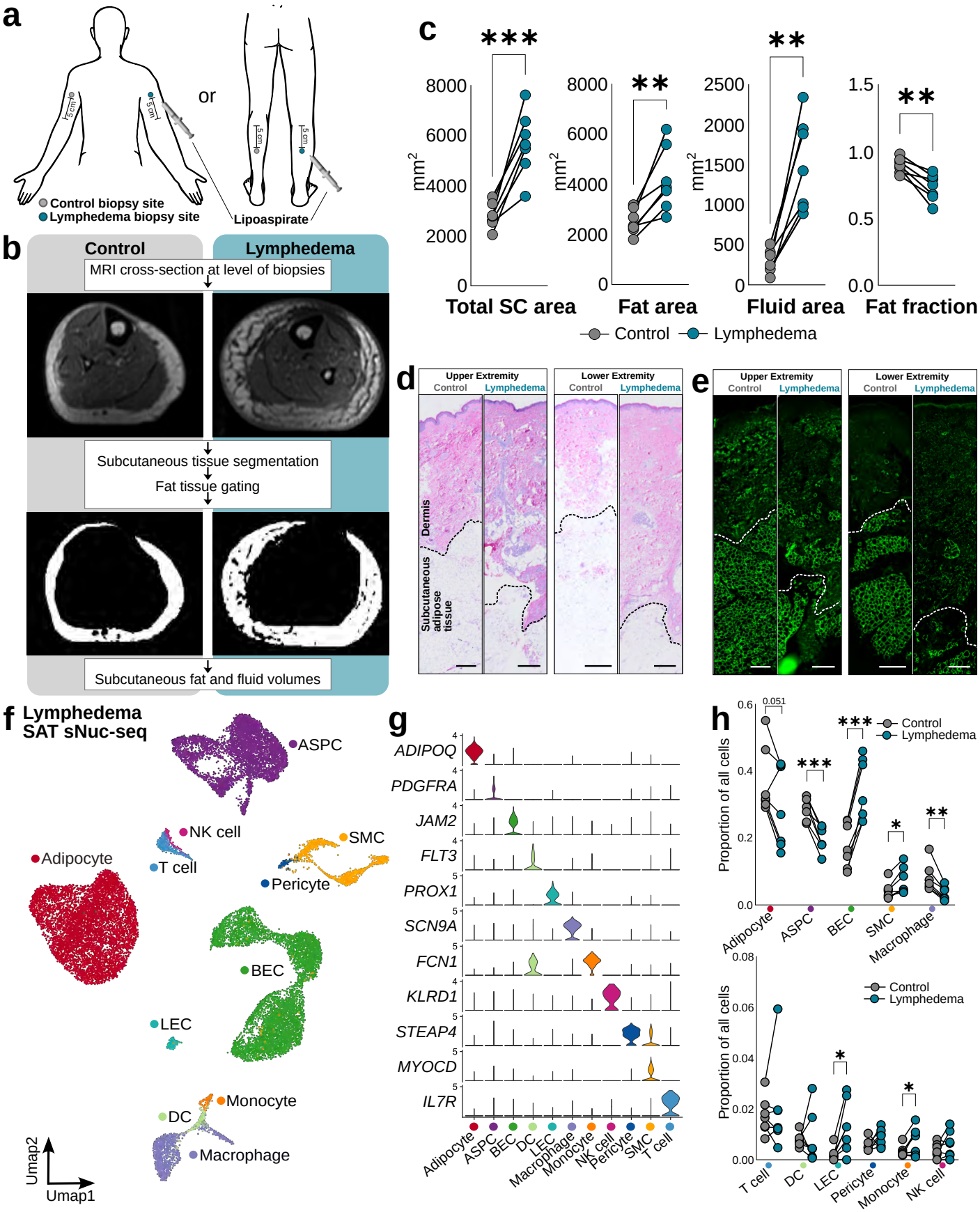
a
or
5 cm
Control biopsy site
Lymphedema biopsy site
Lipoaspirate
b
Control
Lymphedema
MRI cross-section at level of biopsies
Subcutaneous tissue segmentation
Fat tissue gating
Subcutaneous fat and fluid volumes
c
***
**
mm2
Total SC area
Fat area
Fluid area
Fat fraction
Control
Lymphedema
d
Upper Extremity
Lower Extremity
Control
Lymphedema
Dermis
Subcutaneous adipose tissue
e
f Lymphedema SAT sNuc-seq
ASPC
NK cell
SMC
Adipocyte
T cell
Pericyte
BEC
LEC
Monocyte
DC
Macrophage
Umap2
Umap1
g
ADIPOQ
PDGFRA
JAM2
FLT3
PROX1
SCN9A
FCN1
KLRD1
STEAP4
MYOCD
IL7R
Adipocyte
ASPC
BEC
DC
LEC
Macrophage
Monocyte
NK cell
Pericyte
SMC
T cell
h
0.051
Proportion of all cells
Control
Lymphedema
Adipocyte
ASPC
BEC
SMC
Macrophage
T cell
DC
LEC
Pericyte
Monocyte
NK cell

Figure 2

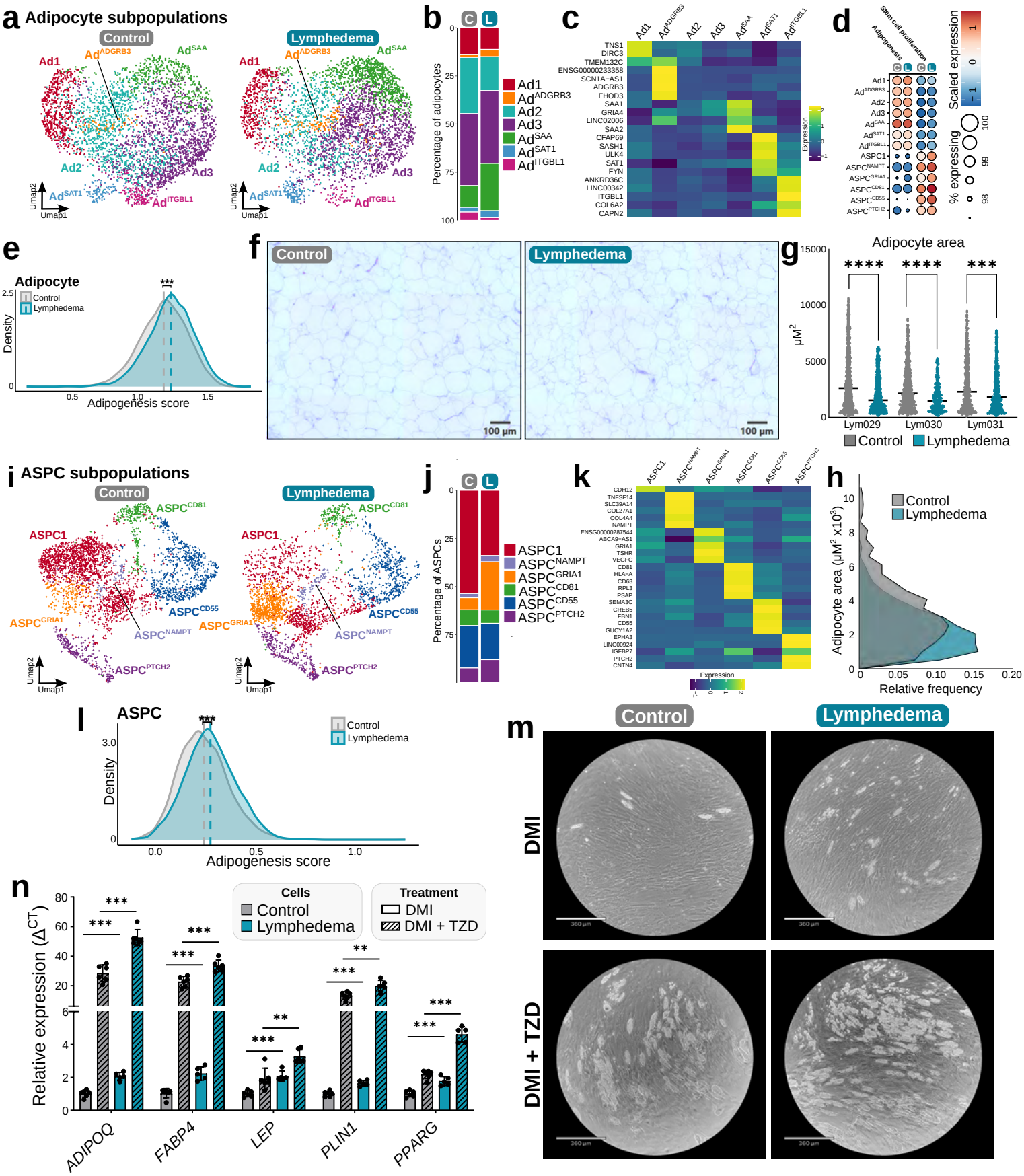
a Adipocyte subpopulations
Control
Lymphedema
Ad1
Ad^ADGRB3
Ad^SAA
Ad2
Ad3
Ad^SAT1
Ad^ITGBL1
Umap1
Umap2
b
C
L
Percentage of adipocytes
Ad1
Ad^ADGRB3
Ad2
Ad3
Ad^SAA
Ad^SAT1
Ad^ITGBL1
c
TNS1
DIRC3
TMEM132C
ENSG00000233358
SCN1A-AS1
ADGRB3
FHOD3
SAA1
GRIA4
LINC02006
SAA2
CFAP69
SASH1
ULK4
SAT1
FYN
ANKRD36C
LINC00342
ITGBL1
COL6A2
CAPN2
Expression
d
Stem cell proliferation
Adipogenesis
Scaled expression
% expressing
ASPC1
ASPC^NAMPT
ASPC^GRIA1
ASPC^CD81
ASPC^CD55
ASPC^PTCH2
e
Adipocyte
Control
Lymphedema
Density
Adipogenesis score
f
Control
Lymphedema
100 µm
g
Adipocyte area
µM²
Lym029
Lym030
Lym031
Control
Lymphedema
i ASPC subpopulations
Control
Lymphedema
ASPC1
ASPC^CD81
ASPC^CD55
ASPC^GRIA1
ASPC^NAMPT
ASPC^PTCH2
Umap1
Umap2
j
Percentage of ASPCs
k
Expression
h
Adipocyte area (µM² x10³)
Relative frequency
l
ASPC
Density
Adipogenesis score
m
Control
Lymphedema
DMI
DMI + TZD
n
Relative expression (ΔCT)
Cells
Control
Lymphedema
Treatment
DMI
DMI + TZD
ADIPOQ
FABP4
LEP
PLIN1
PPARG

Figure 3

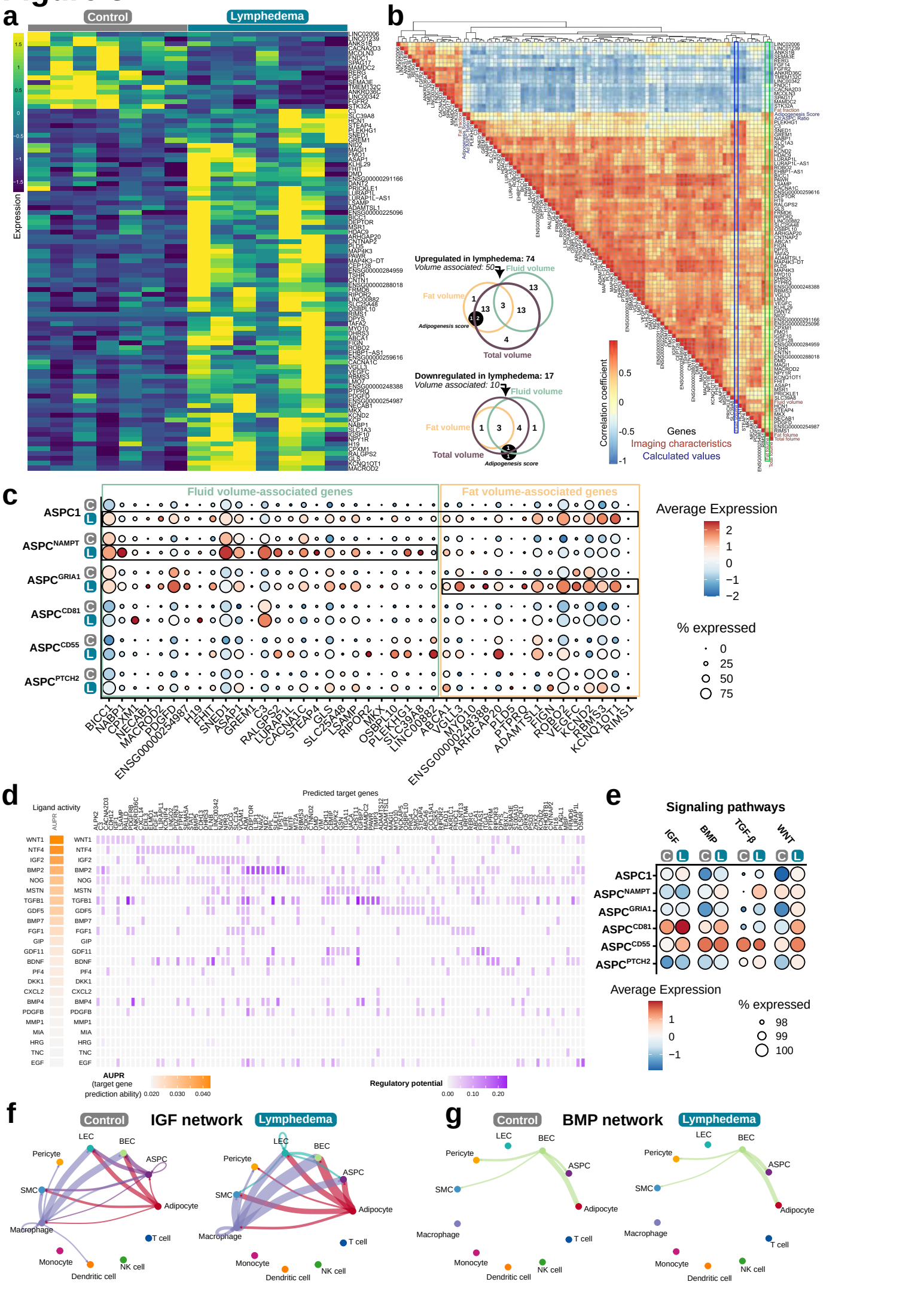
a
Control
Lymphedema
Expression
b
Upregulated in lymphedema: 74
Volume associated: 50
Fluid volume
Fat volume
Adipogenesis score
Total volume
Downregulated in lymphedema: 17
Volume associated: 10
Correlation coefficient
Genes
Imaging characteristics
Calculated values
c
Fluid volume-associated genes
Fat volume-associated genes
ASPC1
ASPC^NAMPT
ASPC^GRIA1
ASPC^CD81
ASPC^CD55
ASPC^PTCH2
Average Expression
% expressed
d
Ligand activity
Predicted target genes
AUPR (target gene prediction ability)
Regulatory potential
e
Signaling pathways
IGF
BMP
TGFβ
WNT
Average Expression
% expressed
f
Control
IGF network
Lymphedema
LEC
BEC
Pericyte
ASPC
SMC
Adipocyte
Macrophage
T cell
Monocyte
NK cell
Dendritic cell
g
Control
BMP network
Lymphedema

Figure 4

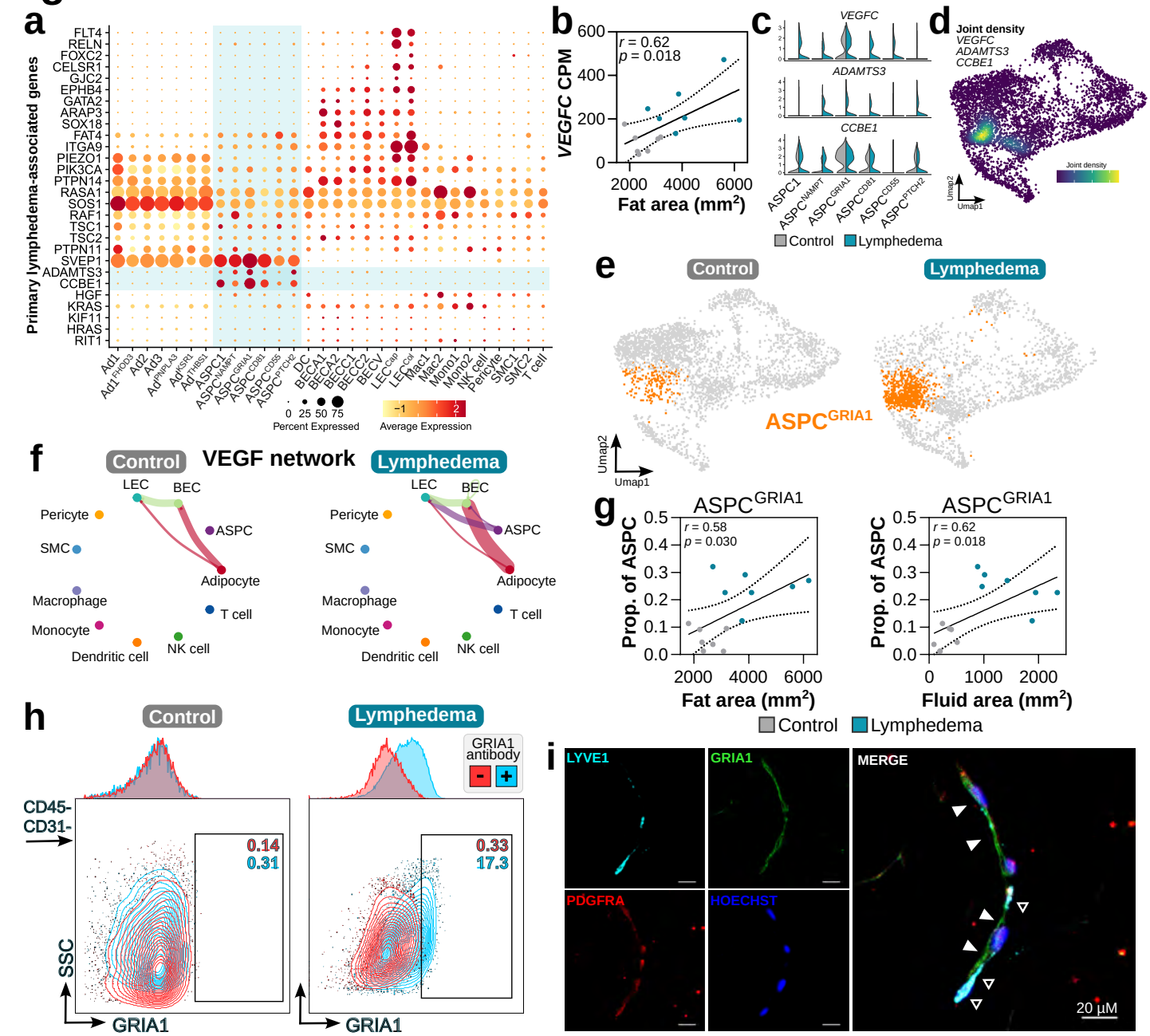
a
Primary lymphedema-associated genes
FLT4
RELN
FOXC2
CELSR1
GJC2
EPHB4
GATA2
ARAP3
SOX18
FAT4
ITGA9
PIEZO1
PIK3CA
PTPN14
RASA1
SOS1
RAF1
TSC1
TSC2
PTPN11
SVEP1
ADAMTS3
CCBE1
HGF
KRAS
KIF11
HRAS
RIT1
Ad1
Ad1 PHOD3
Ad2
Ad3
Ad PNPLA3
Ad KSR1
Ad THBS1
ASPC1
ASPC NAMPT
ASPC GRIA1
ASPC CD81
ASPC CD55
ASPC PTCH2
DC
BECA1
BECA2
BECC1
BECC2
BECV
LEC Cap
LEC Col
Mac1
Mac2
Mono1
Mono2
NK cell
Pericyte
SMC1
SMC2
T cell
0 25 50 75
Percent Expressed
−1 2
Average Expression
b
VEGFC CPM
r = 0.62
p = 0.018
Fat area (mm²)
c
VEGFC
ADAMTS3
CCBE1
ASPC1
ASPC NAMPT
ASPC GRIA1
ASPC CD81
ASPC CD55
ASPC PTCH2
Control
Lymphedema
d
Joint density
VEGFC
ADAMTS3
CCBE1
Joint density
Umap2
Umap1
e
Control
Lymphedema
ASPC GRIA1
Umap2
Umap1
f
Control
VEGF network
Lymphedema
LEC
BEC
Pericyte
ASPC
SMC
Adipocyte
Macrophage
T cell
Monocyte
Dendritic cell
NK cell
g
ASPC GRIA1
r = 0.58
p = 0.030
Prop. of ASPC
Fat area (mm²)
ASPC GRIA1
r = 0.62
p = 0.018
Prop. of ASPC
Fluid area (mm²)
Control
Lymphedema
h
Control
Lymphedema
GRIA1 antibody
CD45-
CD31-
0.14
0.31
0.33
17.3
SSC
GRIA1
GRIA1
i
LYVE1
GRIA1
MERGE
PDGFRA
HOECHST
20 µM

Figure 5

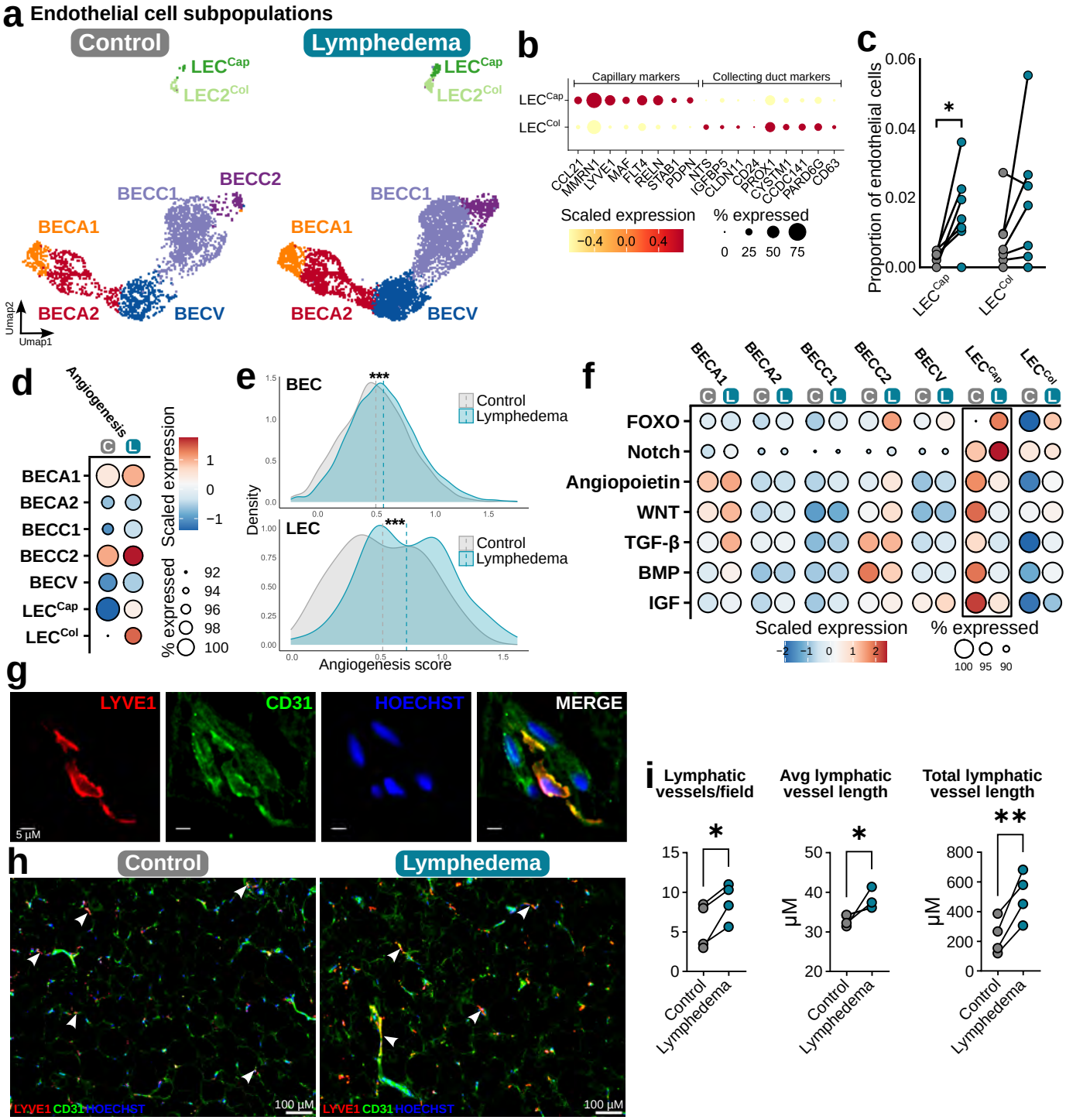
a Endothelial cell subpopulations
Control
Lymphedema
LEC^Cap
LEC2^Col
BECC1
BECC2
BECA1
BECA2
BECV
Umap2
Umap1
b
Capillary markers
Collecting duct markers
LEC^Cap
LEC^Col
CCL21
MMRN1
LYVE1
MAF
FLT4
RELN
STAB1
PDPN
NTS
IGFBP5
CLDN11
CD24
PROX1
CYSTM1
CCDC141
PARD6G
CD63
Scaled expression
% expressed
c
Proportion of endothelial cells
d
Angiogenesis
C
L
Scaled expression
% expressed
e
BEC
LEC
Control
Lymphedema
Density
Angiogenesis score
f
FOXO
Notch
Angiopoietin
WNT
TGF-β
BMP
IGF
Scaled expression
% expressed
g
LYVE1
CD31
HOECHST
MERGE
5 µM
h
Control
Lymphedema
100 µM
i
Lymphatic vessels/field
Avg lymphatic vessel length
Total lymphatic vessel length
µM

Figure 6

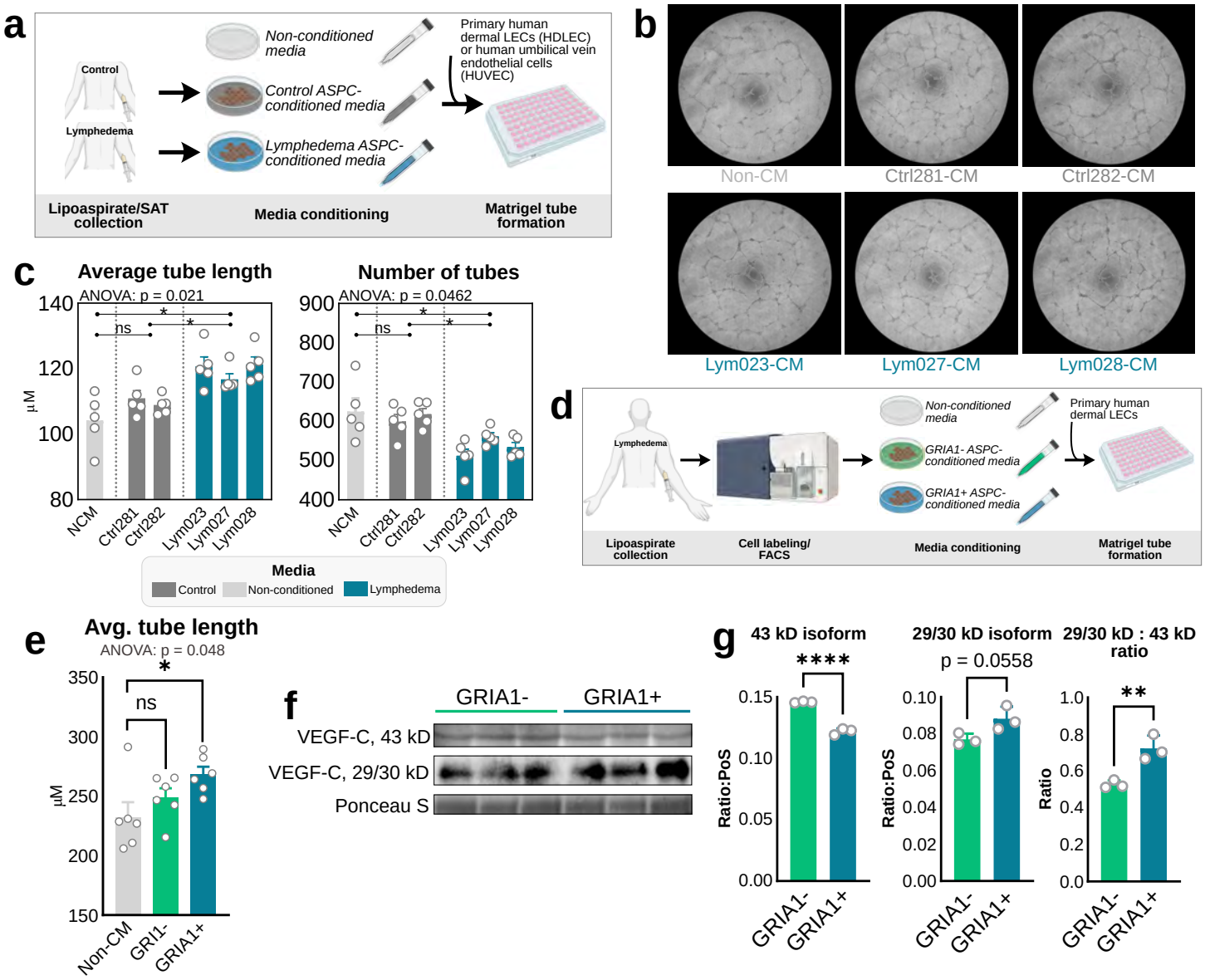
a
Control
Lymphedema
Non-conditioned media
Control ASPC-conditioned media
Lymphedema ASPC-conditioned media
Primary human dermal LECs (HDLEC) or human umbilical vein endothelial cells (HUVEC)
Lipoaspirate/SAT collection
Media conditioning
Matrigel tube formation
b
Non-CM
Ctrl281-CM
Ctrl282-CM
Lym023-CM
Lym027-CM
Lym028-CM
c
Average tube length
ANOVA: p = 0.021
Number of tubes
ANOVA: p = 0.0462
ns
*
μM
NCM
Ctrl281
Ctrl282
Lym023
Lym027
Lym028
Media
Control
Non-conditioned
Lymphedema
d
Lymphedema
Non-conditioned media
GRIA1- ASPC-conditioned media
GRIA1+ ASPC-conditioned media
Primary human dermal LECs
Lipoaspirate collection
Cell labeling/ FACS
Media conditioning
Matrigel tube formation
e
Avg. tube length
ANOVA: p = 0.048
ns
*
μM
Non-CM
GRI1-
GRIA1+
f
GRIA1-
GRIA1+
VEGF-C, 43 kD
VEGF-C, 29/30 kD
Ponceau S
g
43 kD isoform
****
29/30 kD isoform
p = 0.0558
29/30 kD : 43 kD ratio
**
Ratio:PoS
Ratio
GRIA1-
GRIA1+

Extended Data Figure 1

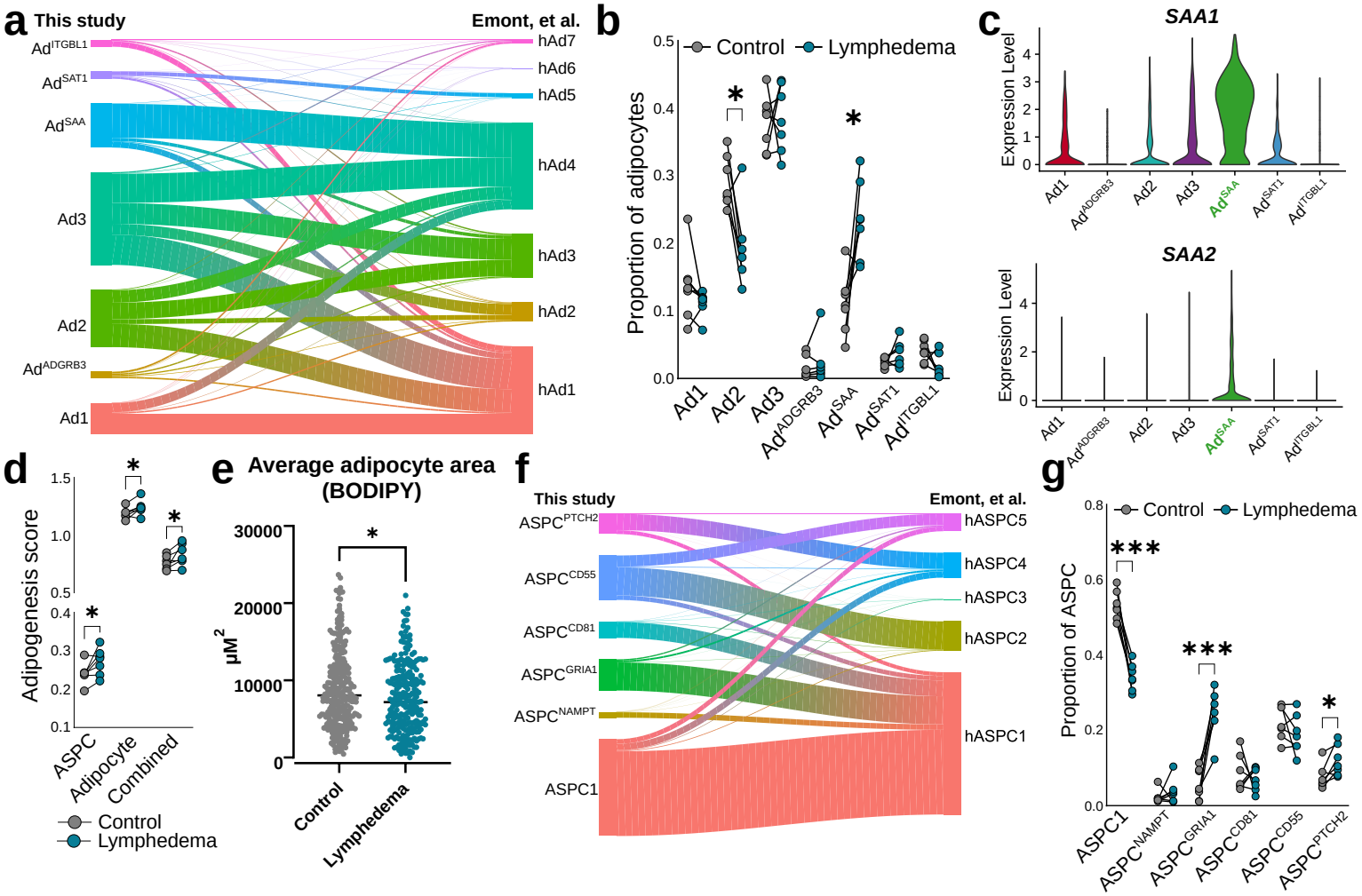

Extended Data Figure 2

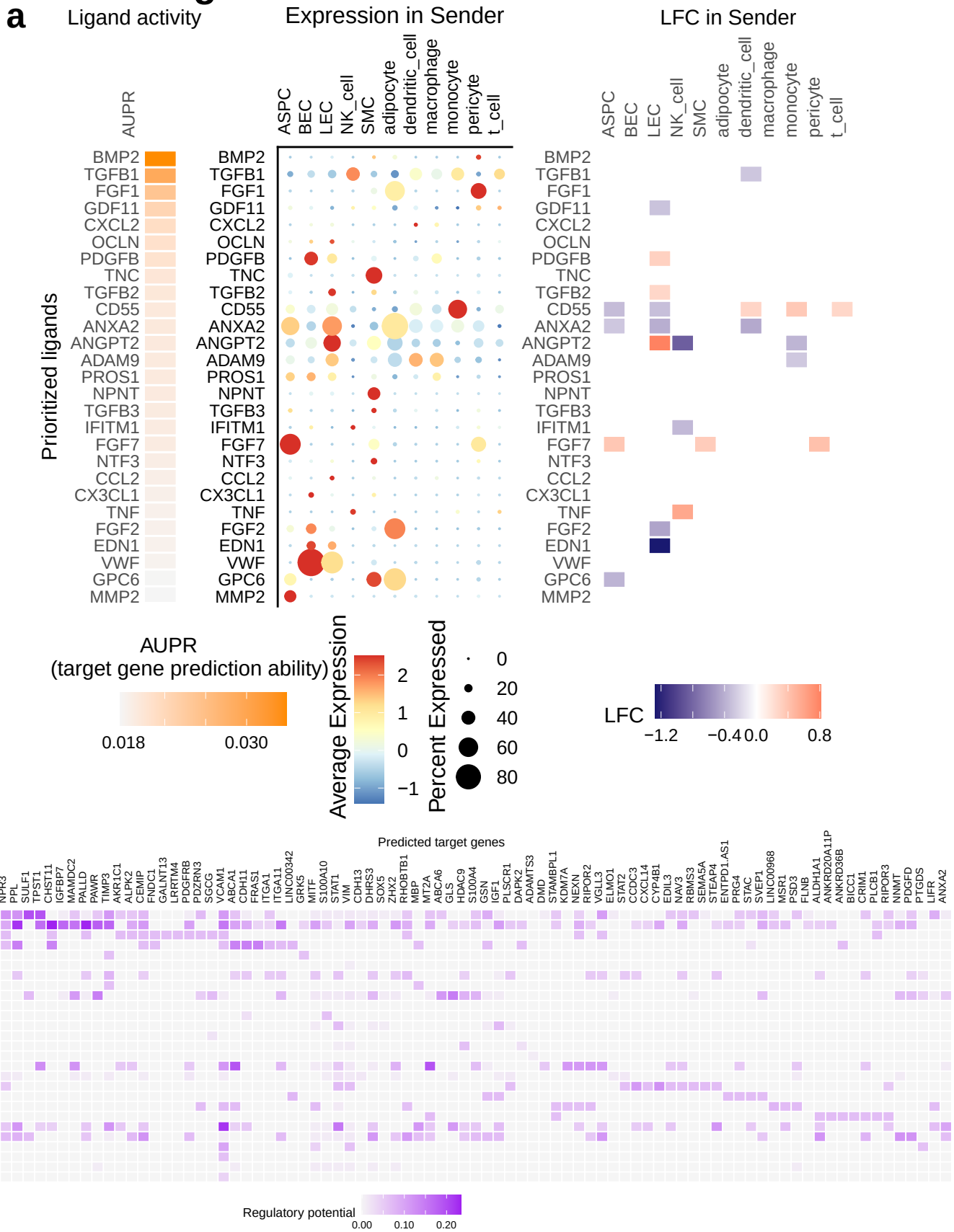

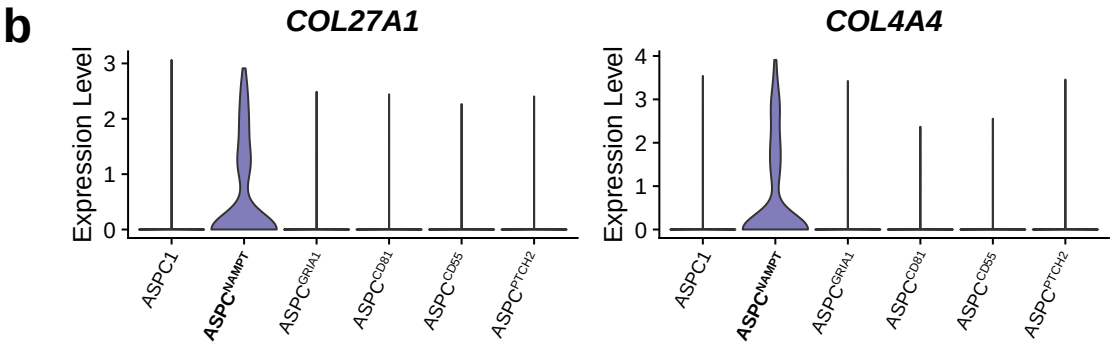

Extended Data Figure 3

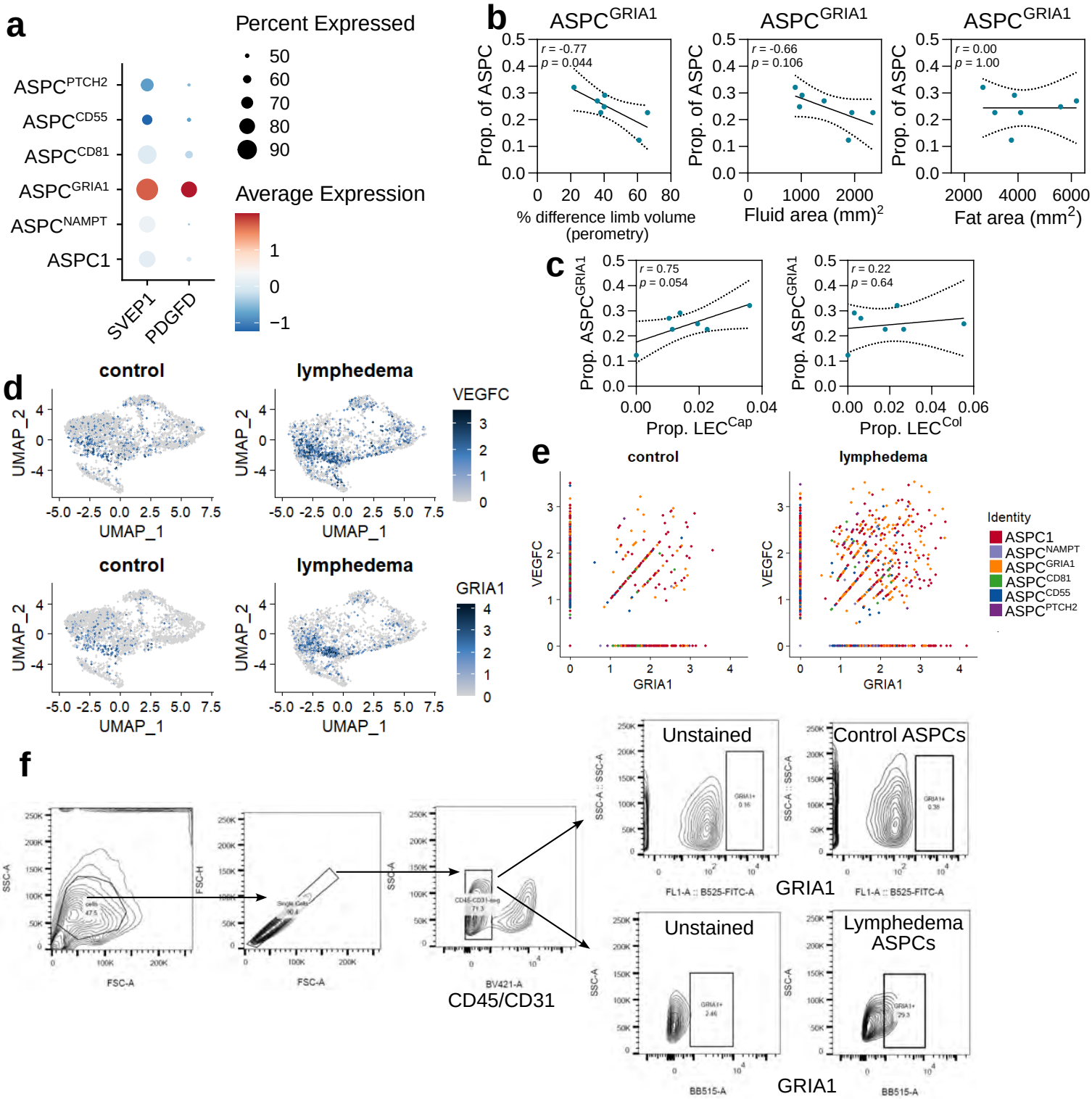

Extended Data Figure 4

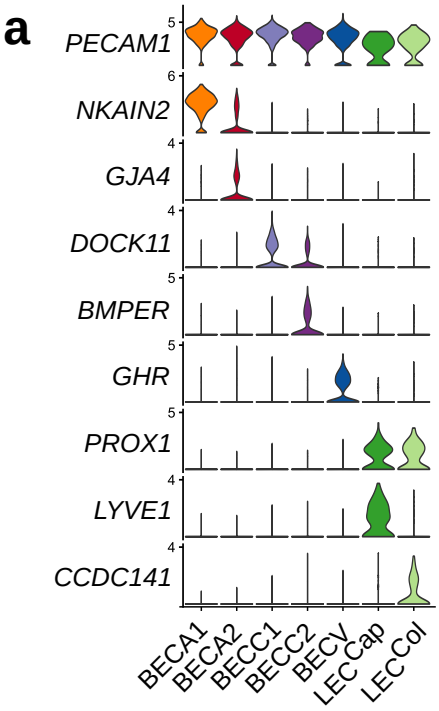

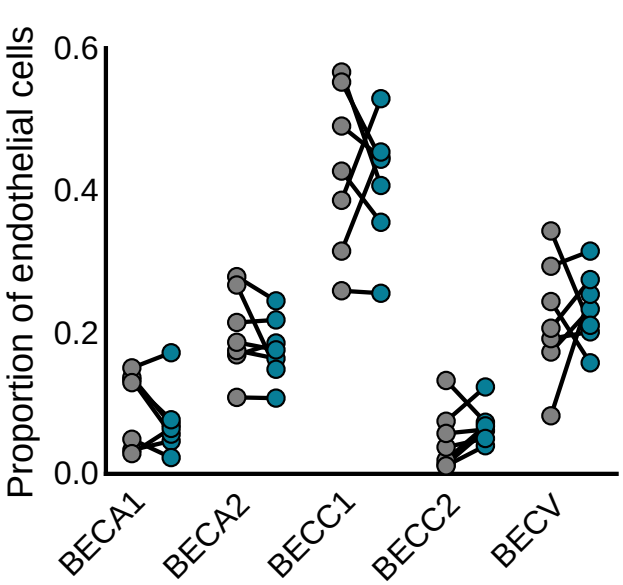

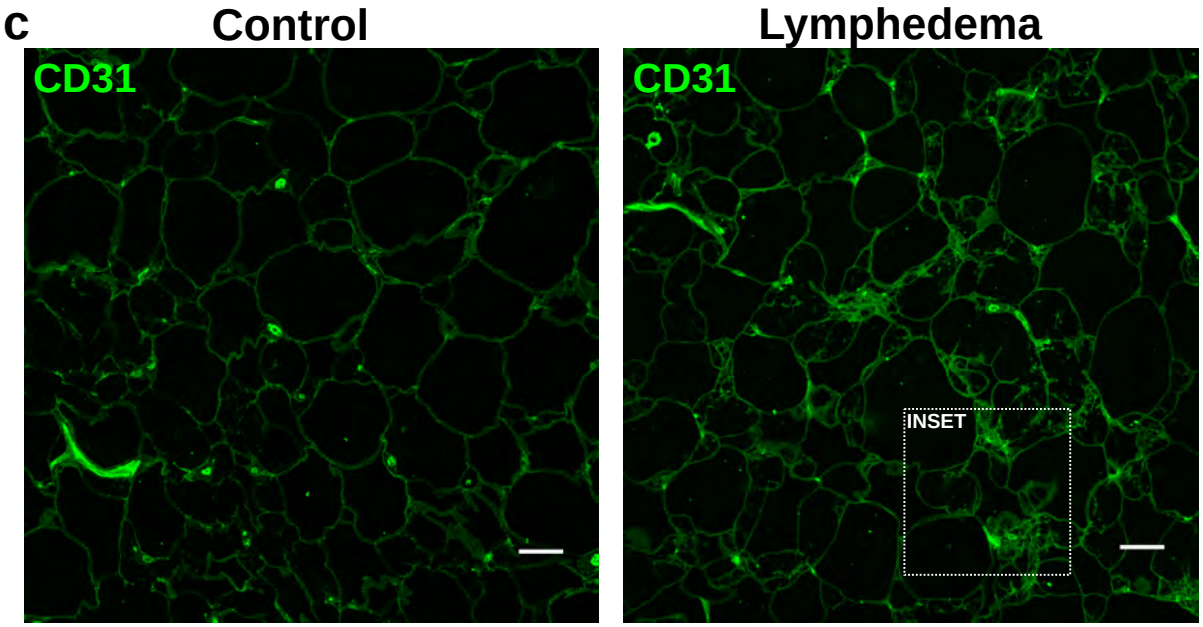

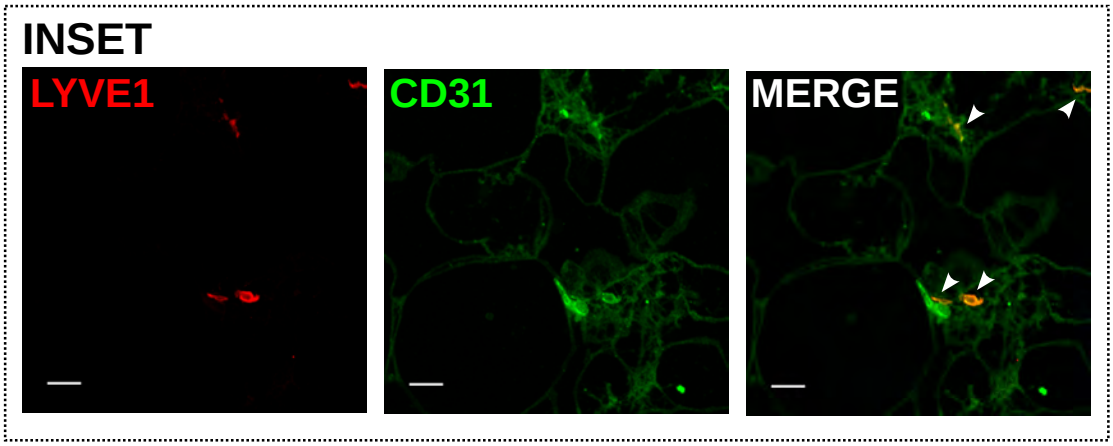
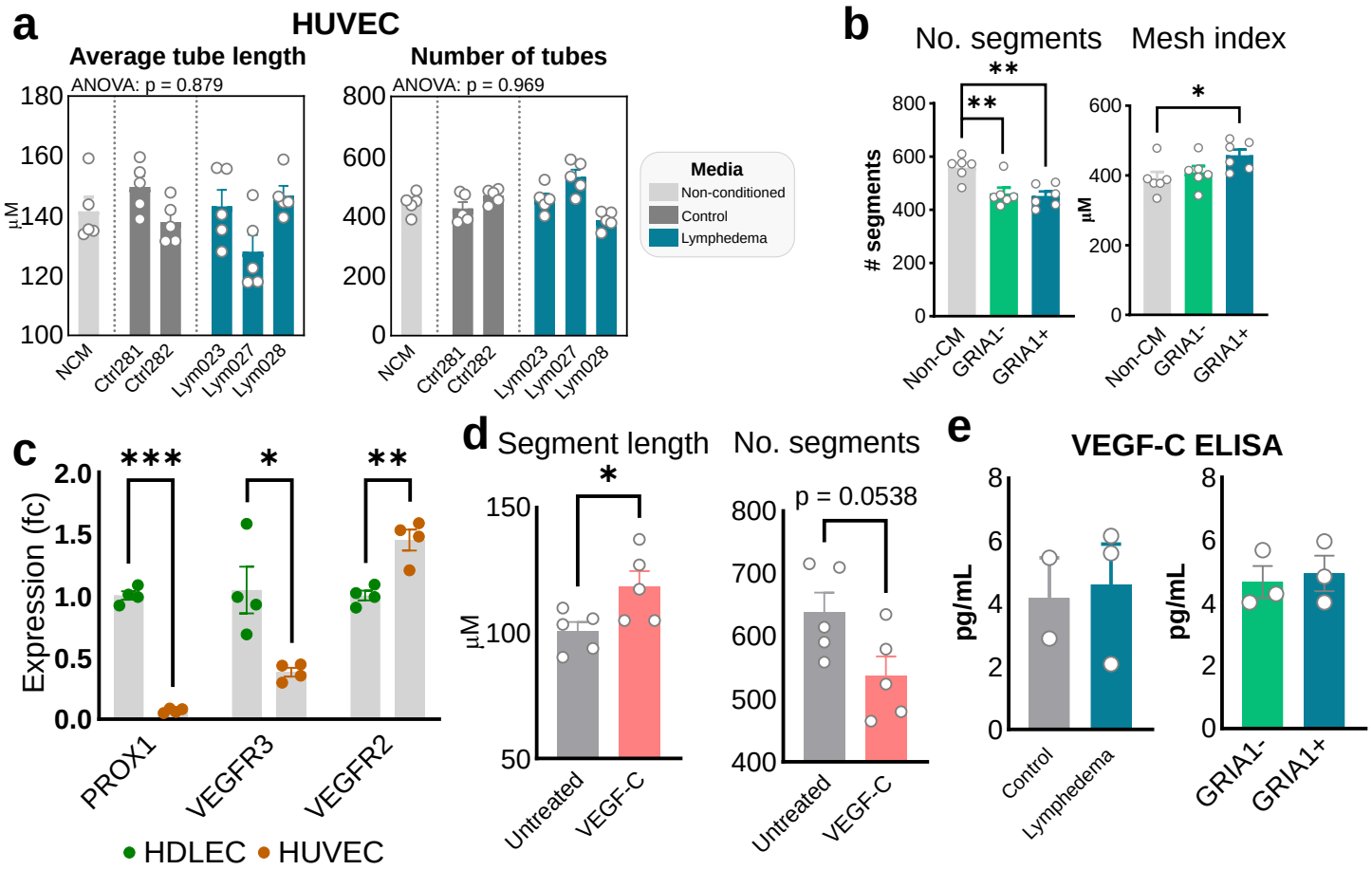
Extended Data Figure 5